Electronic Supporting Information For

Readily available systems for the cycloaddition of CO_2 to epoxides through a water-enhanced application of alkaloid organocatalysts

Yanisa Pongsupradit, [a] Wuttichai Natongchai, [a] Valerio D' Elia, [*a,b]

[a] *Department of Materials Science and Engineering, VISTEC Advanced Laboratory for Environment-Related Inorganic and Organic Syntheses, Vidyasirimedhi Institute of Science and Technology, (VISTEC), Payupnai, Wangchan, Rayong 21210, Thailand. E-mail: valerio.delia@vistec.ac.th*

[b] *Department of Biological and Environmental Sciences and Technologies (DiSTeBA), University of Salento, Lecce, Italy, Email: valerio.delia@unisalento.it*

Table of Contents

S1. General information S2
S2. Experimental procedures S3
S3. Additional catalytic results S8
S4. Characterization of **1@MR** S9
S5. Recycling data of **1@MR** S13
S6. Comparison of catalysts S14
S7. Copies of ^{1}H and ^{13}C NMR S15
S8. Analysis of phases of the reaction mixture and mass balance S46
S9. Supporting references S51

S1. General information

1-Hexene oxide was purchased from Thermo Fisher Scientific. Propylene oxide, epichlorohydrin, styrene oxide, glycidyl phenyl ether, benzyl glycidyl ether, and glycidyl methacrylate were obtained from Tokyo Chemical Industry (TCI). 1,2-Epoxyoctane, glycidyl isopropyl ether, glycidol, quinine, quinuclidine, quinoline, cinchonidine, 6-methoxyquinoline, and mesitylene were purchased from Sigma-Aldrich. Cyclohexene oxide was obtained from Merck. All chemicals were of analytical or reagent grade and were employed as supplied by the manufacturers.

All operations involving air and water sensitive materials were carried out under nitrogen atmosphere using standard Schlenk techniques, or in a nitrogen glovebox. All solvents and reagents were used as received without further purification. Dried solvents were initially dried using a Pure Process Technology solvent purification system. The CO_2 gas (99.995%) was obtained from Bangkok Industrial Gas Company Ltd.

Liquid phase NMR spectra were recorded on a Bruker Avance III spectrometer operating at 600 MHz for H and 150 MHz for C nuclei. Chemical shifts (δ) are reported in parts per million relatives to tetramethylsilane (TMS) and referenced to residual solvent peaks ($CDCl_3$: δ = 7.26 ppm for ^{1}H and 77.16 ppm for ^{13}C; DMSO-d_6: δ = 2.50 ppm for ^{1}H and 39.52 ppm for ^{13}C). Solid state (SS) ^{13}C CP/MAS NMR spectra were measured on a AVANCE III HD/Ascend 400 WB operating at 400 MHz (100.6 MHz for carbon) using 512 scans at a spinning rate of 8000 Hz. Calibration of the SS ^{13}C CP/MAS NMR spectra was done using the glycine peak at 43.3 ppm.

FT-IR spectra were collected using a PerkinElmer Frontier FT-IR spectrometer equipped with a Universal ATR accessory operating in ATR mode.

X-ray photoelectron spectroscopy (XPS) measurements were conducted on a JEOL JPS-9010MC spectrometer using a Mg Kα radiation source (1253.6 eV) operated at 10 kV and 10 mA. All spectra were acquired at room temperature under high vacuum (10^{-8} Pa) and calibrated against the adventitious carbon C 1s peak at 284.80 eV.

Elemental analyses (CHNS) were performed using a LECO TruSpec Micro Elemental Analyzer, calibrated with 2,5-bis(5-tert-butyl-2-benzoxazolyl)thiophene (BBOT) as the standard, with samples loaded in tin capsules.

Scanning electron microscopy (SEM) imaging and elemental mapping were carried out using a JEOL JSM-7610F field-emission scanning electron microscope equipped with an Oxford Instruments energy-dispersive X-ray spectroscopy (EDS) system.

S2. Experimental procedures

General Procedures for Substrates 5a–14a: The epoxide substrate (8.33 mmol) and the catalyst **1** were charged into a 120 mL autoclave equipped with a magnetic stirrer. 0.50 mL of 0.17 M HI solution was added to the mixture. CO_2 was then introduced to the autoclave, and the mixture was stirred for 12 h at 80 °C. After this period, the residual pressure in the reactor was carefully vented, and an aliquot of the reaction mixture was analyzed by ^{1}H NMR spectroscopy in $CDCl_3$ to determine substrate conversion and carbonate selectivity over diol.

Procedure for Substrate 15a: The epoxide substrate **15a** (22.5 mmol) and the catalyst **1** were charged into a 120 mL autoclave equipped with a magnetic stirrer. CO_2 was then introduced to the autoclave, and the mixture was stirred for 12 h at desired temperature. After this period, the residual pressure in the reactor was carefully vented, and an aliquot of the reaction mixture was analyzed by ^{1}H NMR spectroscopy in DMSO-d_6 to determine substrate conversion and carbonate selectivity over glycerol.

Phase Separation and Mass Balance Determination: Upon completion of the reaction, the crude biphasic mixtures (except for substrates **6a** and **7a** that afforded homogeneous mixtures) were physically separated using a glass Pasteur pipette. The denser organic phase (bottom layer) was carefully separated from the aqueous phase (top layer). 40 µL of 1,3,5-trimethylbenzene (TMB) was added to serve as ^{1}H NMR standard. To ensure sample homogeneity (due to some possible residual water droplets), *t*-BuOH was added as a co-solvent. An aliquot of the mixture was diluted with methanol-d4 (MeOD) and analyzed by ^{1}H NMR spectroscopy. For mass balance, the molar amounts of products were calculated from the added moles of TMB (0.2875 mmol) and the products' integral values relative to the 9H signal of the internal standard. For substrates **6a** and **7a**, the ^{1}H NMR determination was carried out directly on an aliquot of the single reaction phase.

Synthesis of catalyst 1@MR: Merrifield resin HL (100–200 mesh, 1.7 mmol Cl/g) was reacted with excess (2 equiv.) quinine in toluene at 100 °C overnight. Following the reaction, the mixture was filtered, and the solid residue was washed thoroughly with ether and dried under vacuum to afford the corresponding polymer-supported quaternary ammonium chloride **1@MR**.

Experimental Procedure for Recycling Study: The catalyst **1@MR** was recovered by cannula filtration and washed with diethyl ether and acetone, then was dried under vacuum for 12 hours before next catalytic reaction.

Calculation of Conversion and Selectivity: The conversion of epoxides **5a-15a** was determined via ^{1}H NMR spectroscopy using **Equation S1.** The calculation was based on the integrals of one of the diastereotopic OCH_2CHR protons in the starting material (H_a) and the corresponding signals in the carbonated product (H_b) and the diol by-product (H_c), as shown in **Scheme S1.**

The selectivity of cyclic carbonate **5b-15b** was determined via ^{1}H NMR spectroscopy using **Equation S2.** The calculation was based on the integrals of the carbonated product (H_b) and the diol by-product (H_c), as shown in **Scheme S1.**

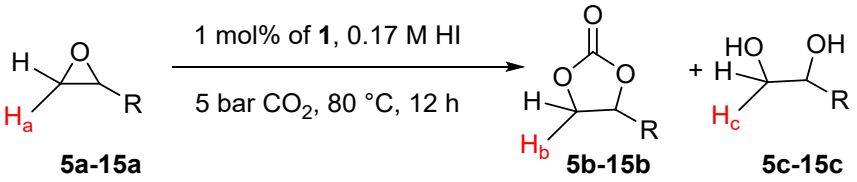

Scheme S1. CO_2 cycloaddition to epoxides into cyclic carbonates

Equation S1. Conversion (%) calculated from the integral values (I) of the OCH_2CHR protons in the starting material (H_a), cyclic carbonate product (H_b) and diol by-product (H_c)

$$\text{Conversion (\%)} = \frac{I_{Hb} + I_{Hc}}{I_{Ha} + I_{Hb} + I_{Hc}} \times 100$$

Equation S2. Selectivity (%) calculated from the integral values (I) of the carbonated product (H_b) and the diol by-product (H_c)

$$\text{Selectivity of cyclic carbonates (\%)} = \frac{I_{Hb}}{I_{Hb} + I_{Hc}} \times 100$$

Table S1. Chemical shifts (δ, ppm) for OCH_2CHR protons and the corresponding carbonated product and diols.

Substrate	δ (H_a) (ppm)	δ (H_b) (ppm)	δ (H_c) (ppm)
5a	2.74	4.48	3.63
6a	2.99	4.55	3.63
7a	2.45	4.59	3.75
8a	2.74	4.52	3.31
9a	3.15	4.80	3.77
10a	2.79	4.48	3.75
11a	2.79	4.63	3.75
12a	2.79	4.61	3.75
13a	2.72	4.94	3.59
14a	3.12	4.67 (*cis*), 3.95 (*trans*)	3.35
15a	2.66	4.29	3.29

Because the cycloaddition of CO_2 to glycidol can lead to the formation of polymeric material,[1] we checked the reactions mass balance by quantifying the moles of glycerol carbonate produced and remaining moles of glycidol by mean of an internal standard (1,3,5-trimethylbenzene)

Calibration curves for glycidol and glycerol carbonate concentrations were constructed by preparing five standard solutions of glycidol and glycerol carbonate at concentrations of 0.4, 1.0, 2.0, 3.0, and 4.0 M. Each standard was prepared by dissolving the appropriate amount of compound in methanol and diluting to volume in a 10 mL volumetric flask. An aliquot (200 µL) of

each solution was transferred to an NMR tube, followed by the addition of 1,3,5-trimethylbenzene (20 μL) as an internal standard and DMSO-d_6 (600 μL) as the solvent.

^{1}H NMR spectra were recorded, and calibration curves were obtained from the ratio of the integral of the three aromatic protons of 1,3,5-trimethylbenzene at 6.74 ppm to that of the characteristic glycidol proton at approximately 2.66 ppm (H_A, **Figure S1**) or the glycerol carbonate proton at 4.29 ppm (H_B, **Figure S3**), as shown in **Figures S2 and S4**, respectively.

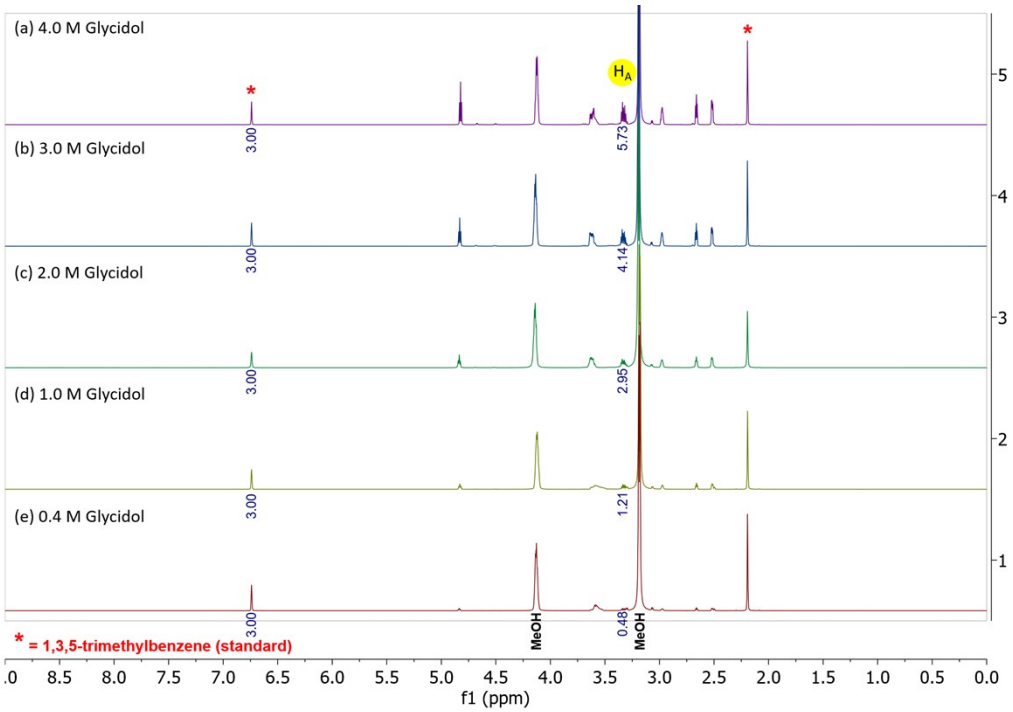

Figure S1. ^{1}H NMR spectra for glycidol calibration in DMSO-d_6 (δ 2.50 ppm) by addition of 1,3,5-trimethylbenzene as a standard (*).

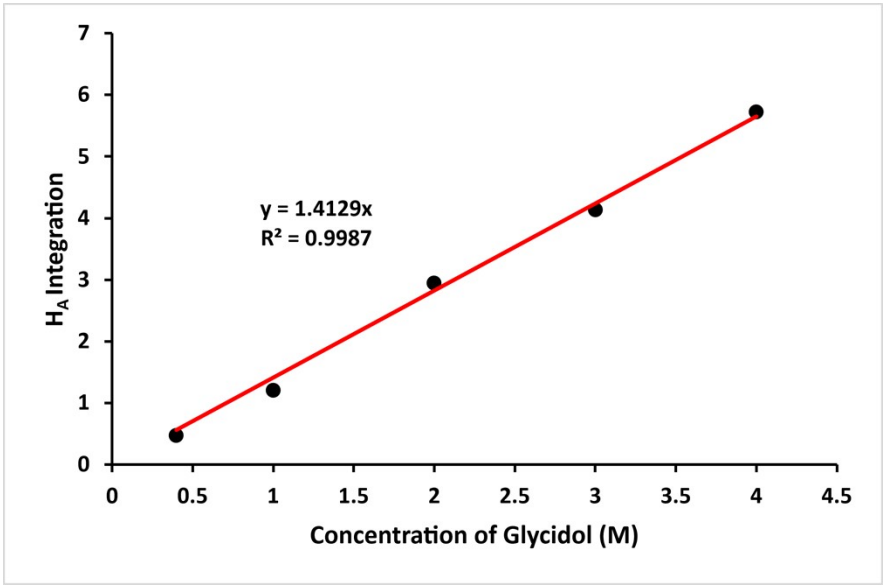

Figure S2. ^{1}H NMR calibration curve for glycidol concentration based on the integral ratio of the aromatic protons of 1,3,5-trimethylbenzene at 6.74 ppm (3H) to the glycidol proton at approximately 2.66 ppm (H_A).

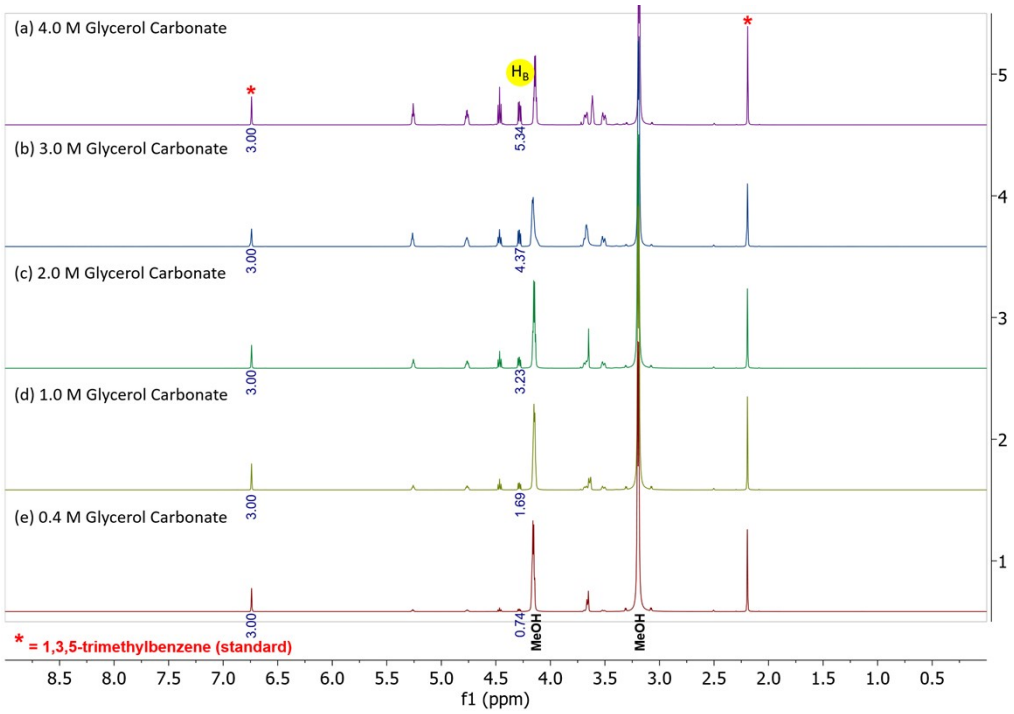

Figure S3. ^{1}H NMR spectra for glycerol carbonate calibration in DMSO-d_6 (δ 2.50 ppm) by addition of 1,3,5-trimethylbenzene as a standard (*).

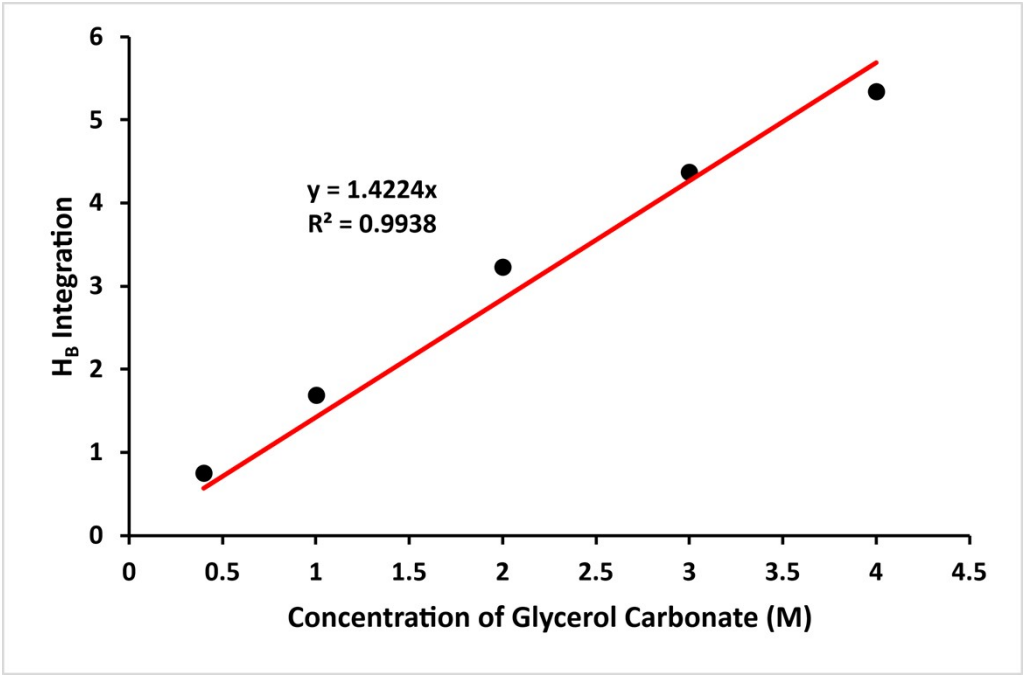

Figure S4. ^{1}H NMR calibration curve for glycerol carbonate concentration based on the integral ratio of the aromatic protons of 1,3,5-trimethylbenzene at 6.74 ppm (3H) to the glycerol carbonate proton at approximately 4.29 ppm (H_B).

To determine the reactions mass balance at the end of the reaction, the crude reaction mixture was diluted with methanol in a 10 mL volumetric flask. A 200 µL aliquot of this solution was transferred to an NMR tube, followed by the addition of DMSO-d_6 (600 µL) and 1,3,5-trimethylbenzene (20 µL) as the internal standard. In the resulting ^{1}H NMR spectrum, the integration of the internal standard's aromatic protons at 6.74 ppm was calibrated to 3.00. The residual glycidol concentration was determined by integrating the characteristic signal at 2.66 ppm (I_{HA}) and dividing the resulting value by the slope of the corresponding calibration curve (1.4129). The concentration of the formed glycerol carbonate was calculated analogously using the integrated intensity of its characteristic signal and the slope of its calibration curve (1.4129). This value was then compared to the initial substrate concentration (2.25 M) to quantify the reactions mass balance as shown in **Equation S3.**

Equation S3. The reaction mass balance (%) was calculated by comparing the total number of moles present before and after the reaction.

$$\text{Reaction mass balance (\%)} = \left(\frac{\frac{I_{HA}}{1.4129} + \frac{I_{HB}}{1.4224}}{2.25} \right) \text{x } 100$$

S3. Additional catalytic results

Table S2. Control experiments and effect of water volume on the cycloaddition of CO_2 to 1-hexene oxide (**5a**).[a]

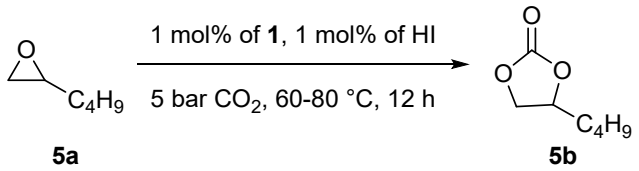

5a **5b**

Entry	Quinine loading (mol%)	Volume of added water (mL)	Conc. HI in added water (M)	Temp. (°C)	Conv. (%)	Select. (%)[b]
1[c]	-	0.5	0.17	80	0	0
2[c]	1	0.5	-	80	0	0
3[d]	1	0.5	0.17	80	> 99	> 99
4[c]	1	0.25	0.34	60	58	> 99
5[e]	1	0.5	0.17	60	74	> 99
6[c]	1	1	0.085	60	76	> 99
7[c]	1	2	0.043	60	19	> 99

[a] 8.33 mmol **5a** (1 mL), **1** (when added), water, HI (1 mol%, when added), at 5 bar CO_2,12 h. [b] Selectivity for cyclic carbonate versus diol product. [c] ^{1}H NMR spectra of the organic phases are given in Figures S65-S69. [d] Taken from Table 1, Entry 7. [e] Taken from Table 1, Entry 8.

S4. Characterization of 1@MR

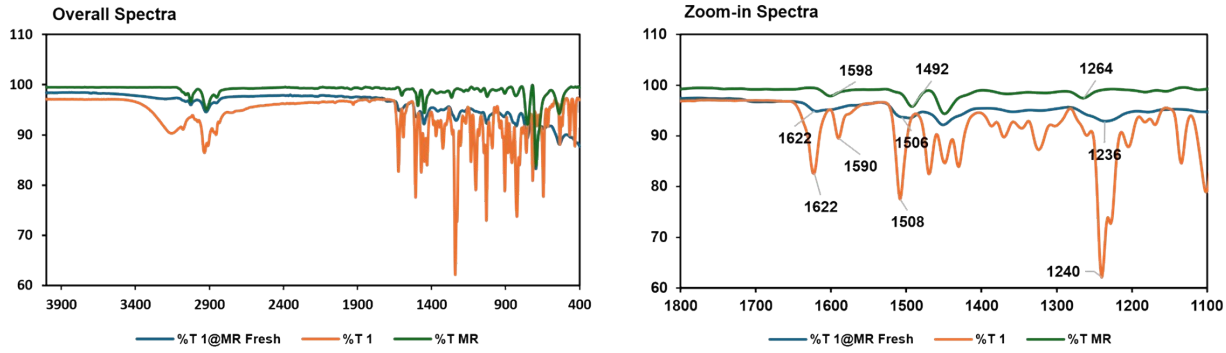

Figure S5. FT-IR Spectra of **1@MR** fresh (blue), **1** (orange), and Merrifield Resin (green). The overall spectrum is given on the left and the detail in the 1100-1800 cm^{-1} region is given in the right.

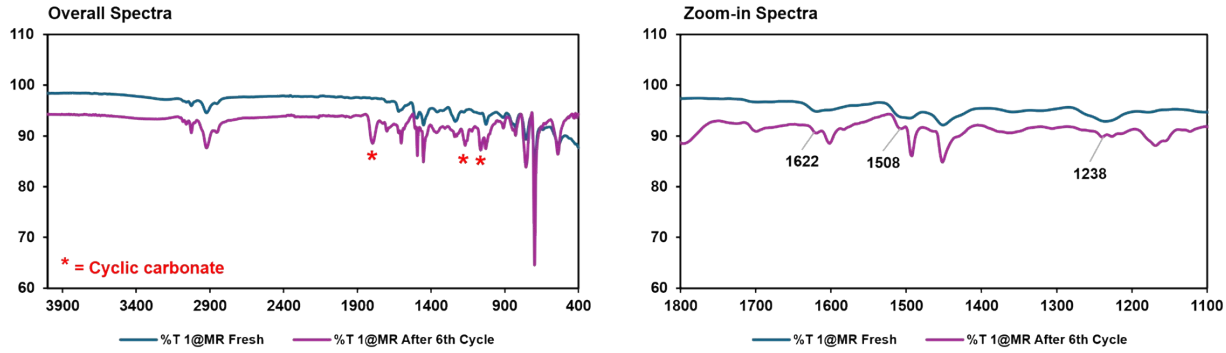

Figure S6. FTIR spectra of **1@MR** after 6th catalytic cycles (purple, the red asterisks indicate the presence of adsorbed cyclic carbonate) compared to fresh **1@MR** (green). The detail on the right shows the presence of the typical quinine signals at 1622, 1508, 1238 cm^{-1} in the spent catalyst.

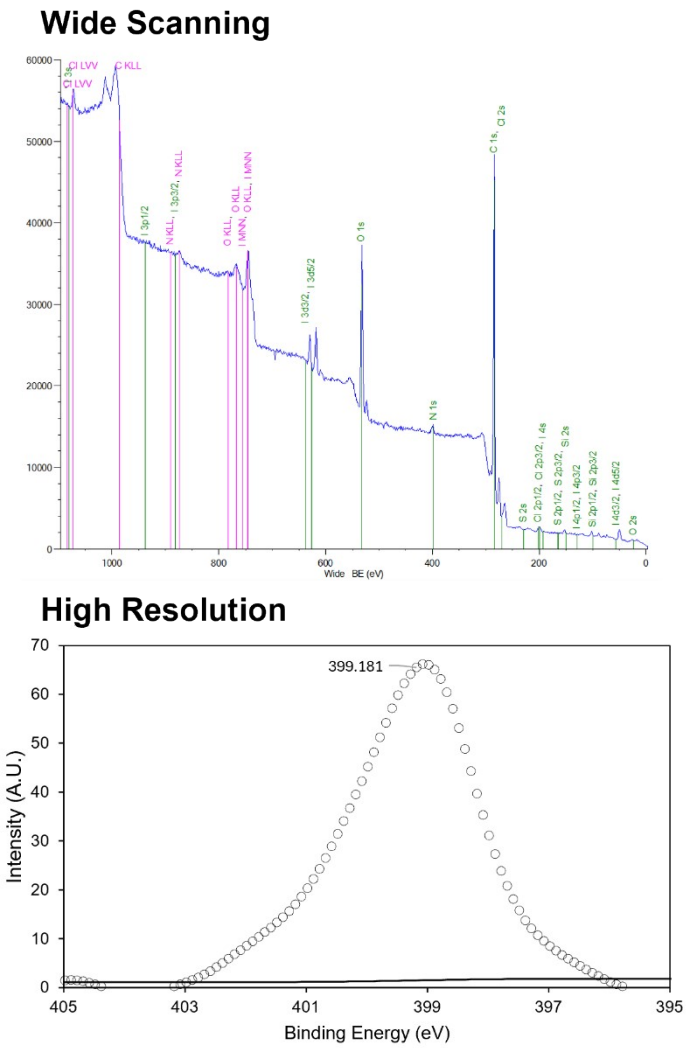

Figure S7. Wide scanning (Top) and High resolution (Bottom) XPS of **1@MR** in the N 1s spectral regions

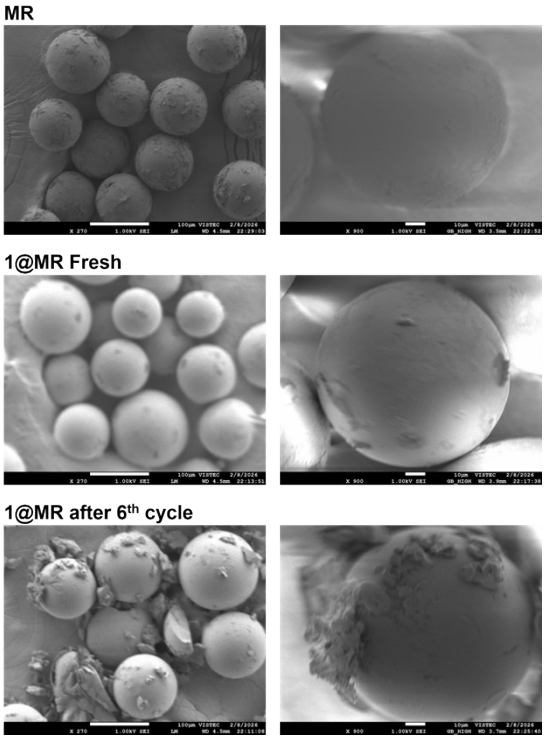

Figure S8. SEM images of polystyrene beads morphology in Merrifield resin (Top), **1@MR** Fresh (Middle) and **1@MR** after 6th cycle (Bottom)

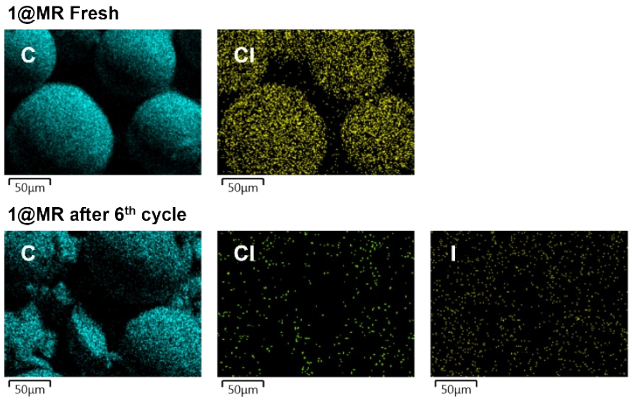

Figure S9. SEM-EDS images of **1@MR** Fresh (Top), and **1@MR** after 6th cycle (Bottom)

Table S3. EDS Analysis of elements in fresh and spent **1@MR**

Element[a]	**Wt%**	
	1@MR Fresh	**1@MR after 6th cycle**
C	96.51	92.70
Cl	3.49	0.10
I	-	7.20
Total	100.00	100.00

[a] It was not possible to observe nitrogen by this technique due to its relatively low concentration.

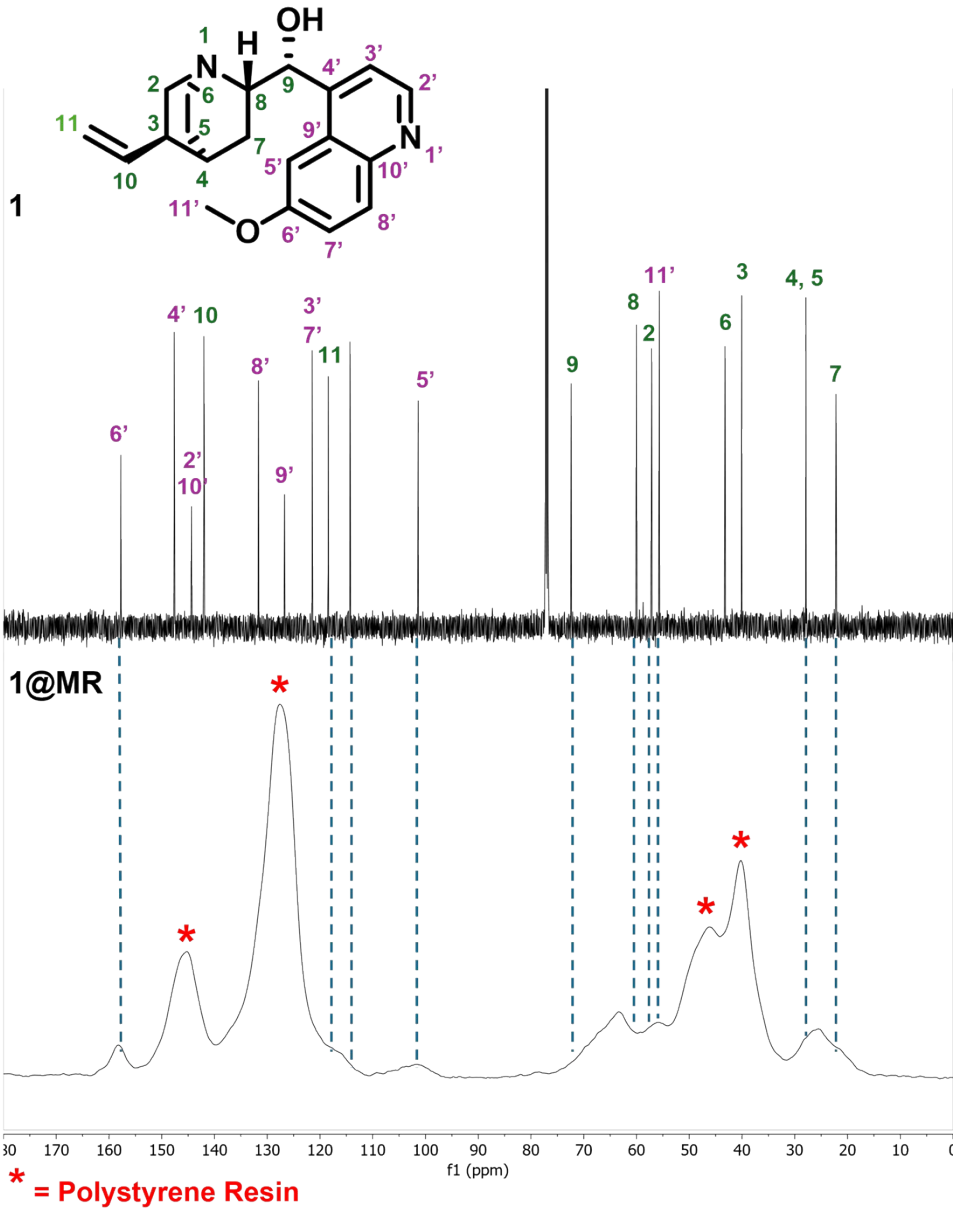

Figure S10. ^{13}C NMR ($CDCl_3$) of **1** (Top) and solid state ^{13}C CP/MAS NMR of **1@MR** (Bottom).

For the attribution of the quinine signals see: Mostafa et al. *Appl. Sci.* **2022**, *12*, 978.

For the attribution of the polystyrene support signals see: Conte et al. *J. Mater. Chem.* **2007**, *17,* 201–205; Law et al. *Macromolecules* **1996,** *29,* 6284-6293.

S5. Recycling data of 1@MR

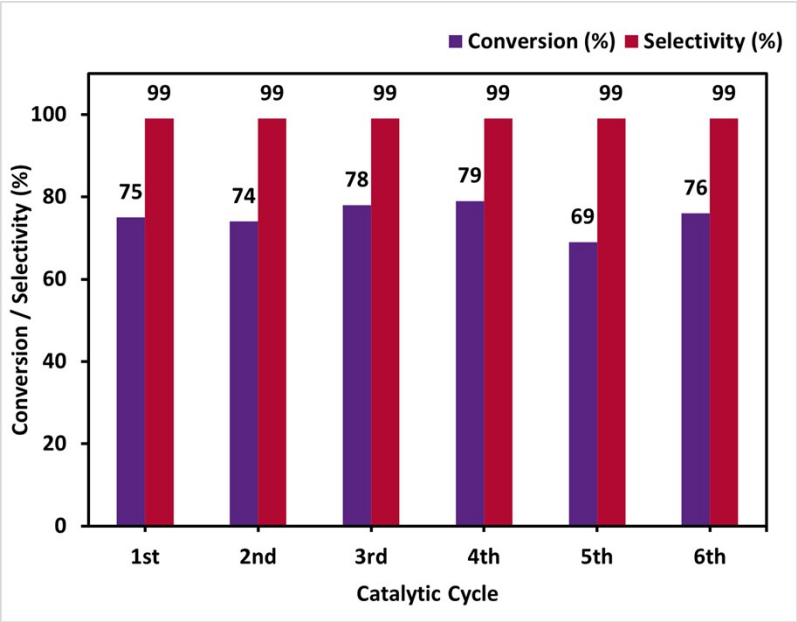

Figure S11. Recycling performance of **1@MR** over six cycles for the cycloaddition of CO_2 to **5a**. Epoxide (8.33 mmol), **1@MR** (50 mg, corresponding to 0.051 mmol or 0.6 mol% **1**), 0.5 mL of 0.17 M HI, 5 bar CO_2, 12 h.

S6. Comparison of catalysts

Table S4. Comparison of catalysts applied under solventless conditions for the cycloaddition of CO_2 to 1-hexene oxide.

Catalyst	Loading (mg) (mol%)[a]	Temp. (°C)	Pressure (bar)	Time (h)	Conv. (%)	TOF (h^{-1})[b]	Select. (%)	Ref.
Al-Gh	80 1.8[a,c]	85	1	24	50	1.2	n.a.	[2]
SnO_2-NPs	100[d] 0.5[a]	80	5	24	66	5.5	>99	[3]
ZIF-8T[b]	50	80	1	48	100		n.a.	[4]
RhB-EtOH-I	1[a]	60	10	24	52	2.2	>99	[5]
HIP-Br-His[e]	100 4.8[a,f]	70	10	24	93	0.8	99	[6]
PMP-TDNs-MI	63.3	110	10	30	95		91	[7]
(1@MR)·HI	50 0.6[a]	80	5	12	75	10.4	>99	This work
(1@MR)·HI	100 1.2[a]	80	5	12	90	6.3	>99	This work

[a] Loading of halide nucleophile. [b] Turnover frequencies calculated as (mol product)/(mol halide nucleophile)(reaction time (h)). [c] Calculated on the basis of 43 wt% guanidinium hydrochloride loading provided in the original manuscript. [d] With the addition of homogeneous 0.5 mol% TBAI. [e] 1-butene oxide as the substrate. [f] Value not provided in the original manuscript and calculated assuming equimolar histidine and α,α'-dibromo-p-xylene ratio in the catalyst.

Al-Gh: guanidine-grafted γ-alumina

ZIF-8T: ZIF-8 framework with 1,2,4-triazole

RhB-EtOH-I: rhodamine B functionalized with hydroxyethoxy iodide

HIP-Br-His: histidine-based hypercrosslinked polymer

PMP-TDNs-MI: melamine and 4,5-imidazoledicarboxylic acid network

S7. Copies of ^{1}H and ^{13}C NMR

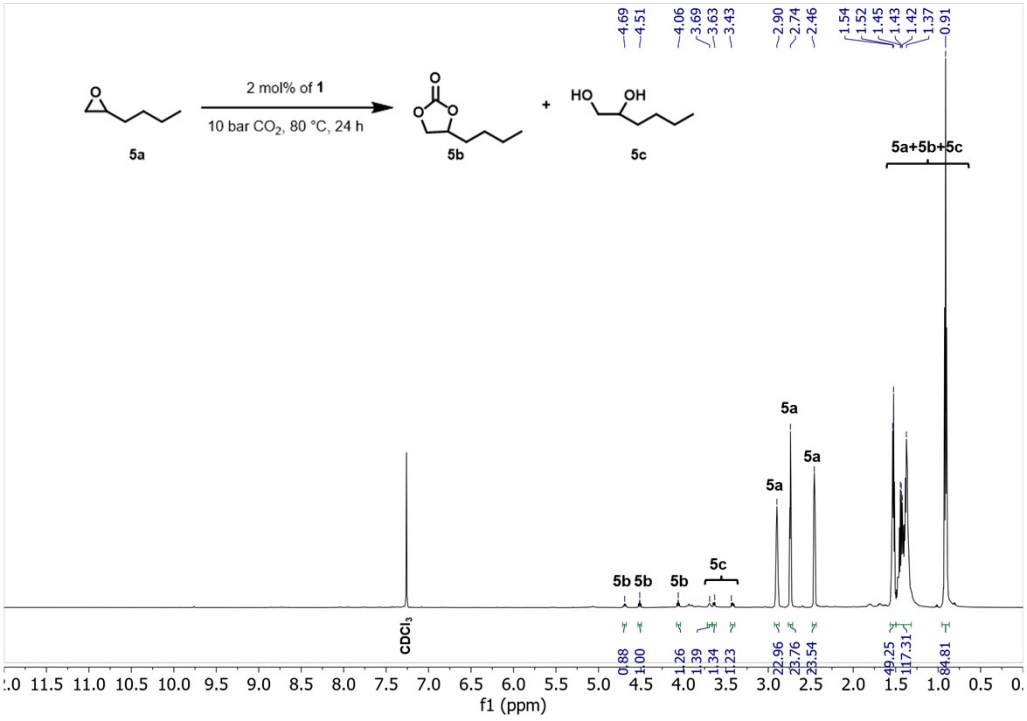

Figure S12. Crude ^{1}H NMR ($CDCl_3$) spectrum of cycloaddition of CO_2 to **5a** substrate by using 2 mol% of **1**, 10 bar CO_2, 80 °C, 24 h; **Table 1, Entry 1**

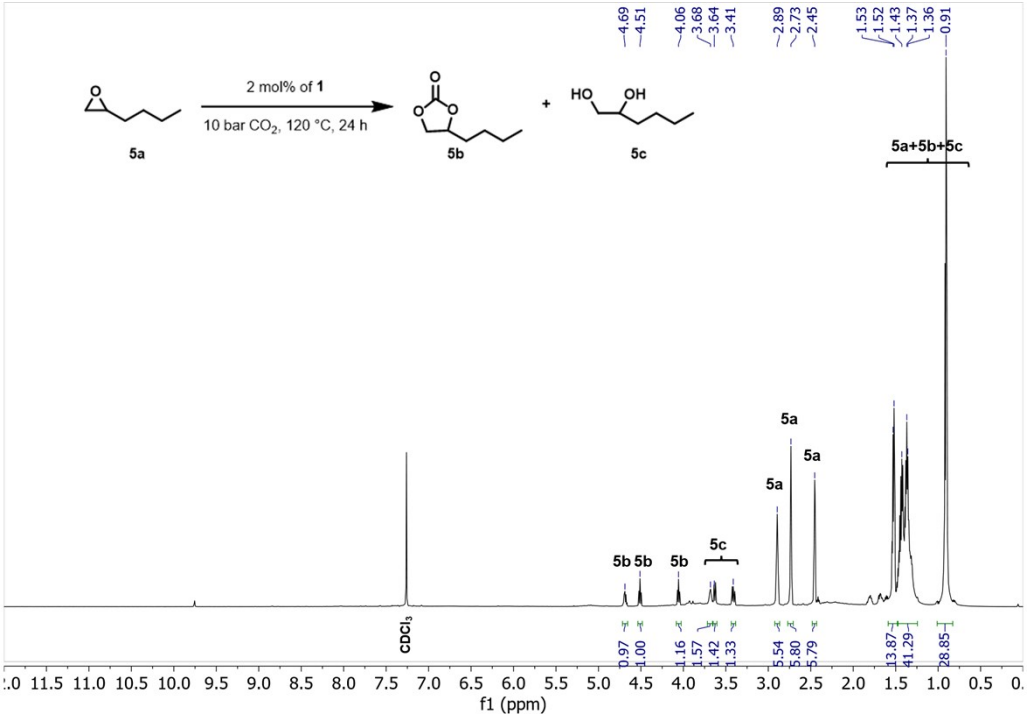

Figure S13. Crude ^{1}H NMR ($CDCl_3$) spectrum of cycloaddition of CO_2 to **5a** substrate by using 2 mol% of **1**, 10 bar CO_2, 120 °C, 24 h; **Table 1, Entry 2**

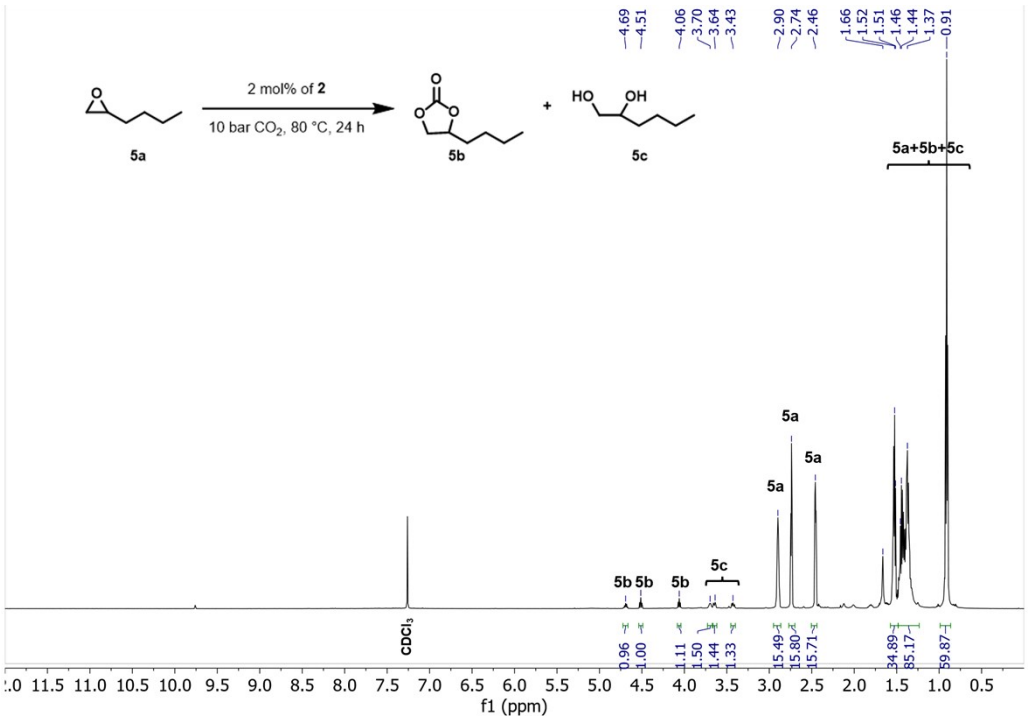

Figure S14. Crude ^{1}H NMR ($CDCl_3$) spectrum of cycloaddition of CO_2 to **5a** substrate by using 2 mol% of **2**, 10 bar CO_2, 80 °C, 24 h; **Table 1, Entry 3**

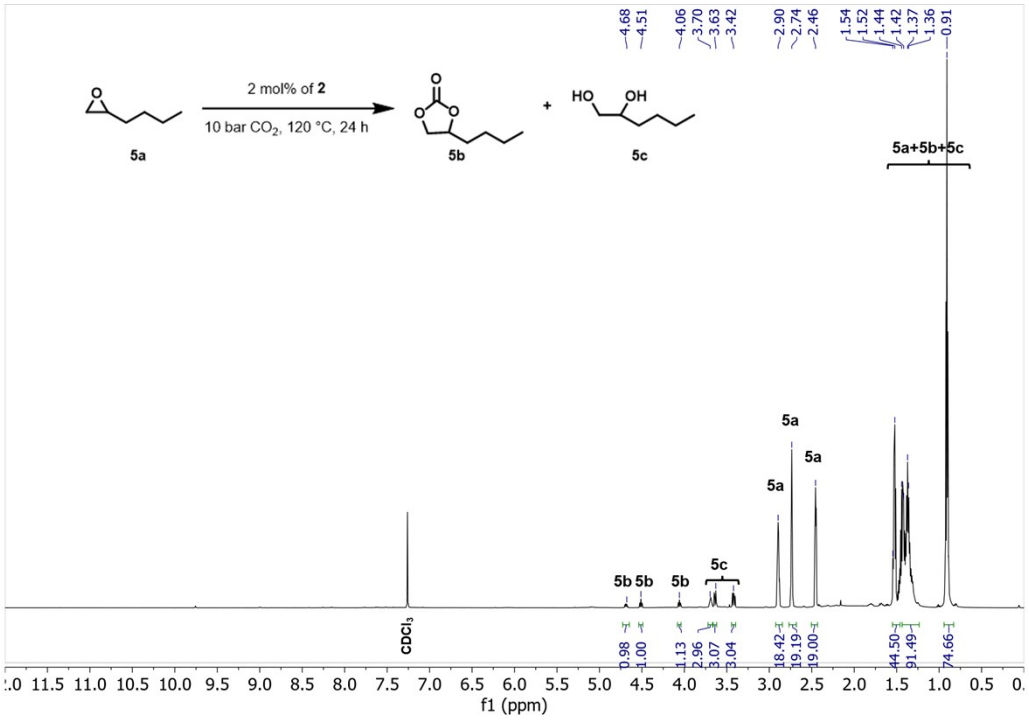

Figure S15. Crude ^{1}H NMR ($CDCl_3$) spectrum of cycloaddition of CO_2 to **5a** substrate by using 2 mol% of **2**, 10 bar CO_2, 120 °C, 24 h; **Table 1, Entry 4**

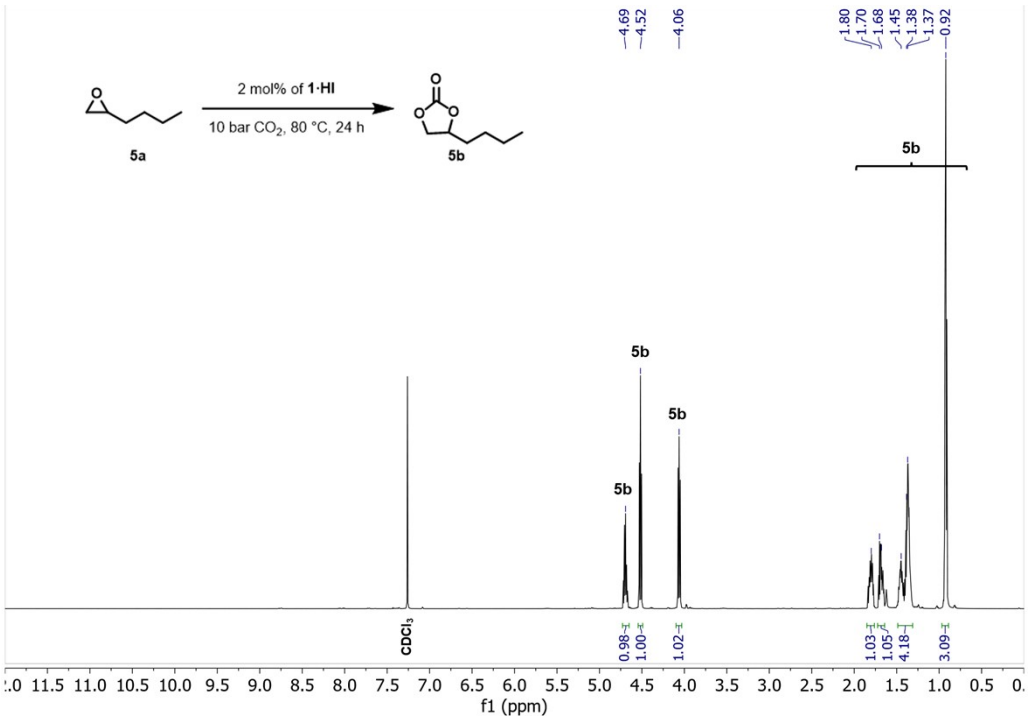

Figure S16. Crude ^{1}H NMR ($CDCl_3$) spectrum of cycloaddition of CO_2 to **5a** substrate by using 2 mol% of **1·HI**, 10 bar CO_2, 80 °C, 24 h; **Table 1, Entry 5**

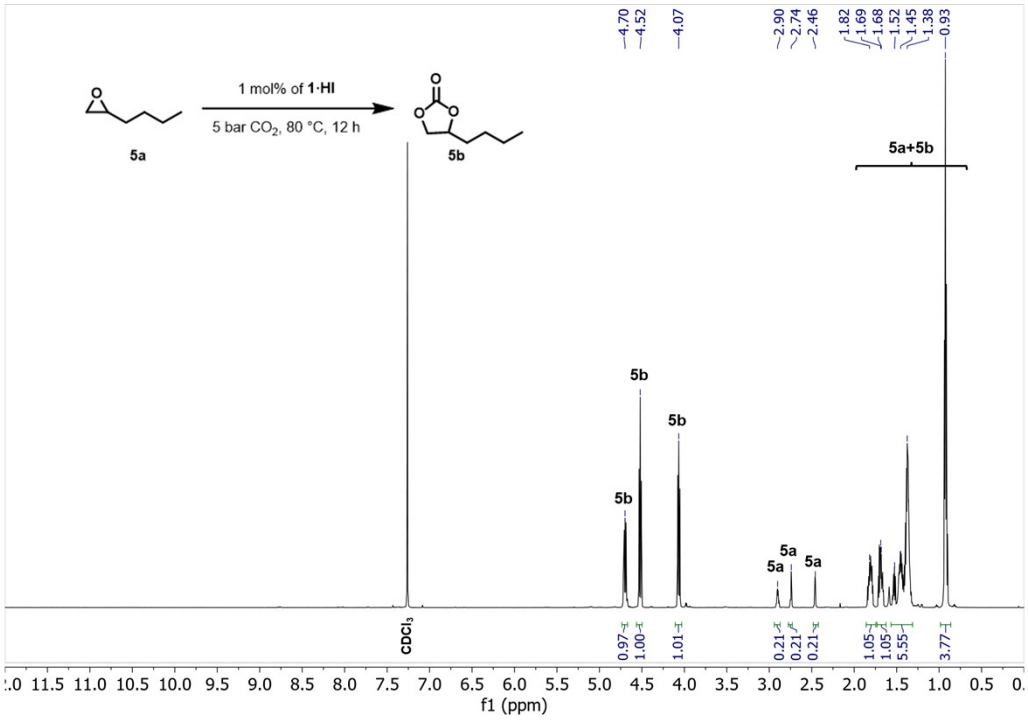

Figure S17. Crude ^{1}H NMR ($CDCl_3$) spectrum of cycloaddition of CO_2 to **5a** substrate by using 1 mol% of **1·HI**, 5 bar CO_2, 80 °C, 12 h; **Table 1, Entry 6**

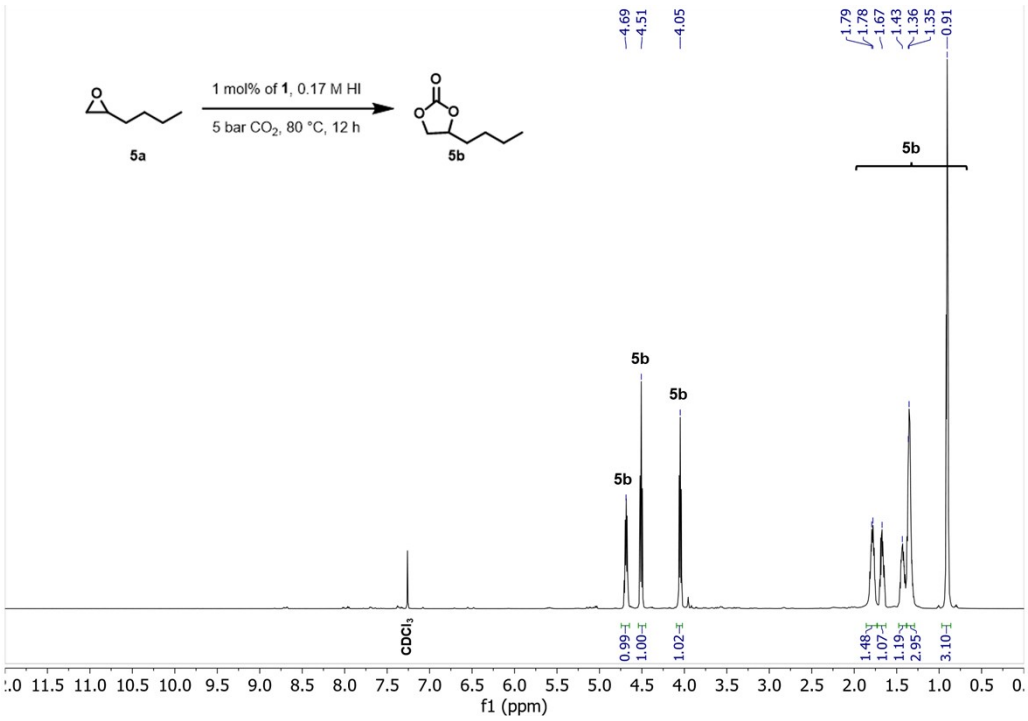

Figure S18. Crude ^{1}H NMR ($CDCl_3$) spectrum of cycloaddition of CO_2 to **5a** substrate by using 1 mol% of **1**, 0.5 mL of 0.17 M HI, 5 bar CO_2, 80 °C, 12 h; **Table 1, Entry 7**

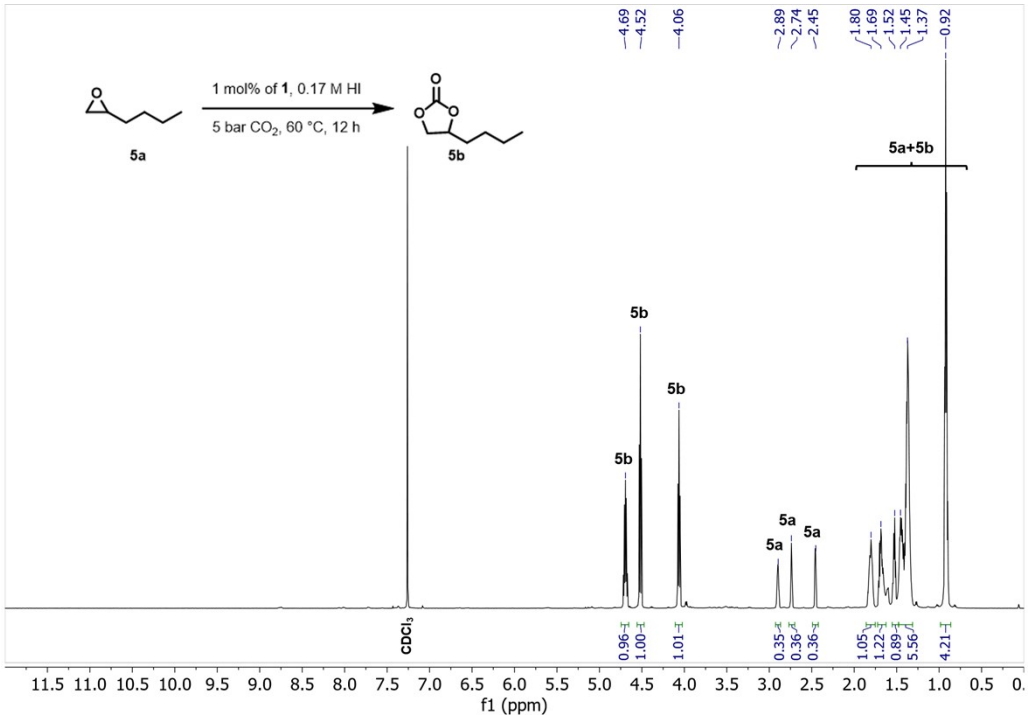

Figure S19. Crude ^{1}H NMR ($CDCl_3$) spectrum of cycloaddition of CO_2 to **5a** substrate by using 1 mol% of **1**, 0.5 mL of 0.17 M HI, 5 bar CO_2, 60 °C, 12 h; **Table 1, Entry 8**

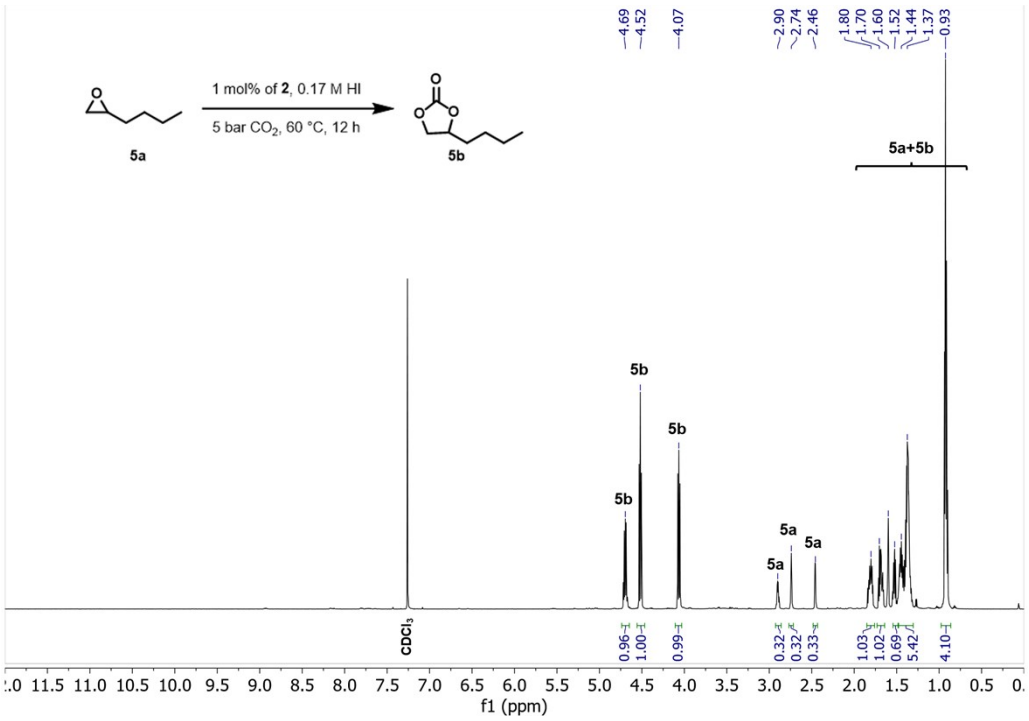

Figure S20. Crude ^{1}H NMR ($CDCl_3$) spectrum of cycloaddition of CO_2 to **5a** substrate by using 1 mol% of **2**, 0.5 mL of 0.17 M HI, 5 bar CO_2, 60 °C, 12 h; **Table 1, Entry 9**

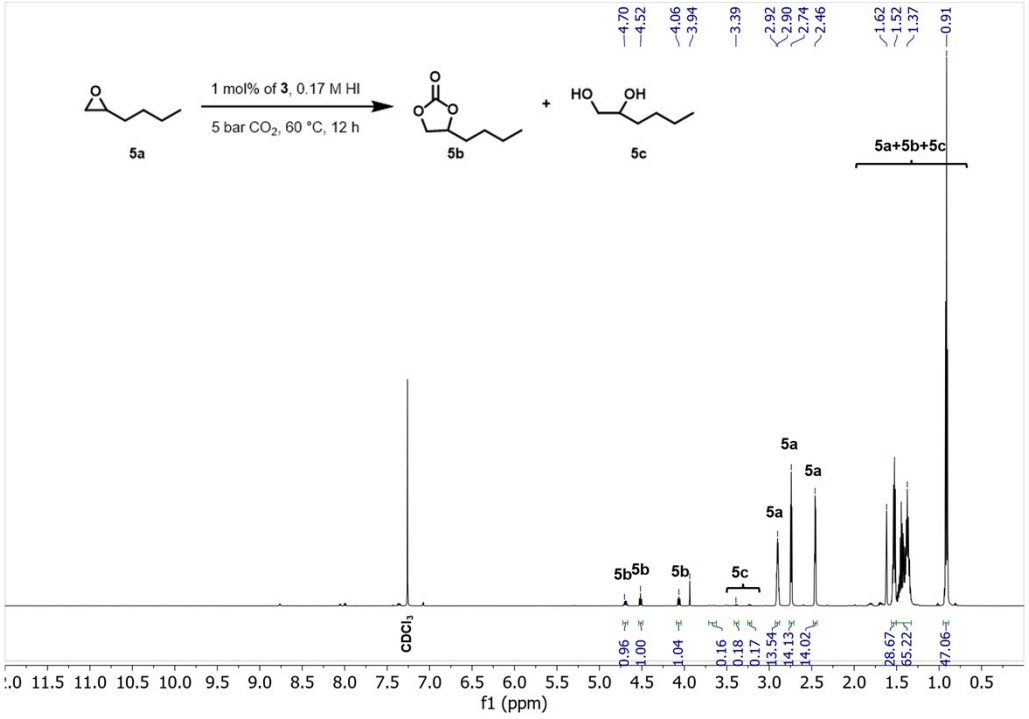

Figure S21. Crude ^{1}H NMR ($CDCl_3$) spectrum of cycloaddition of CO_2 to **5a** substrate by using 1 mol% of **3**, 0.5 mL of 0.17 M HI, 5 bar CO_2, 60 °C, 12 h; **Table 1, Entry 10**

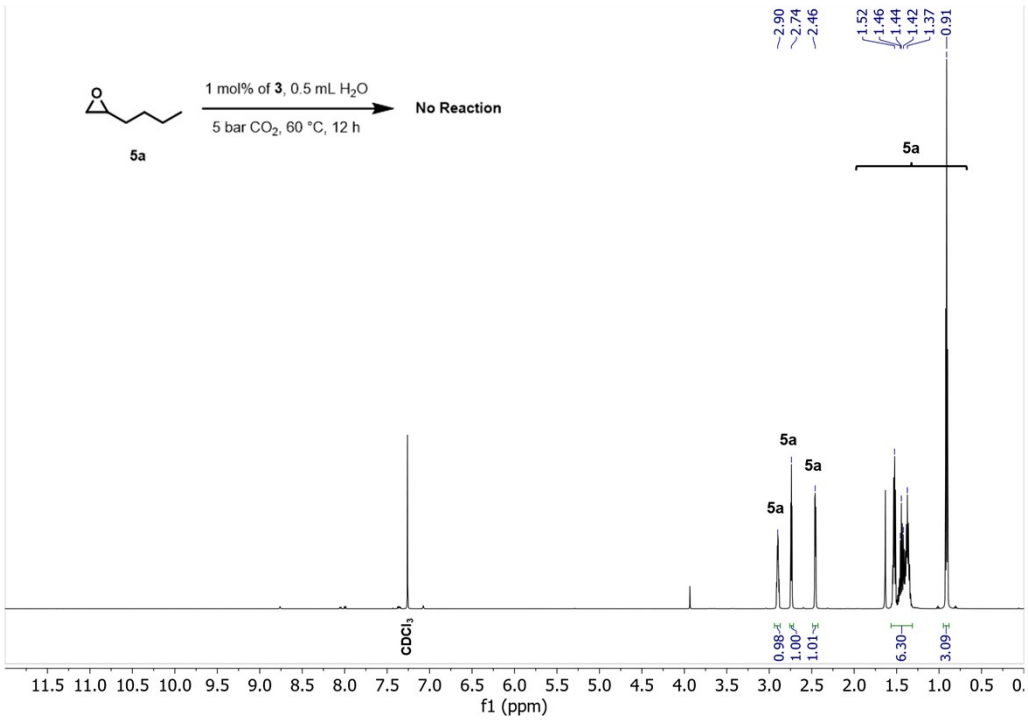

Figure S22. Crude ^{1}H NMR ($CDCl_3$) spectrum of cycloaddition of CO_2 to **5a** substrate by using 1 mol% of **3**, 0.5 mL H_2O, 5 bar CO_2, 60 °C, 12 h; **Table 1, Entry 11**

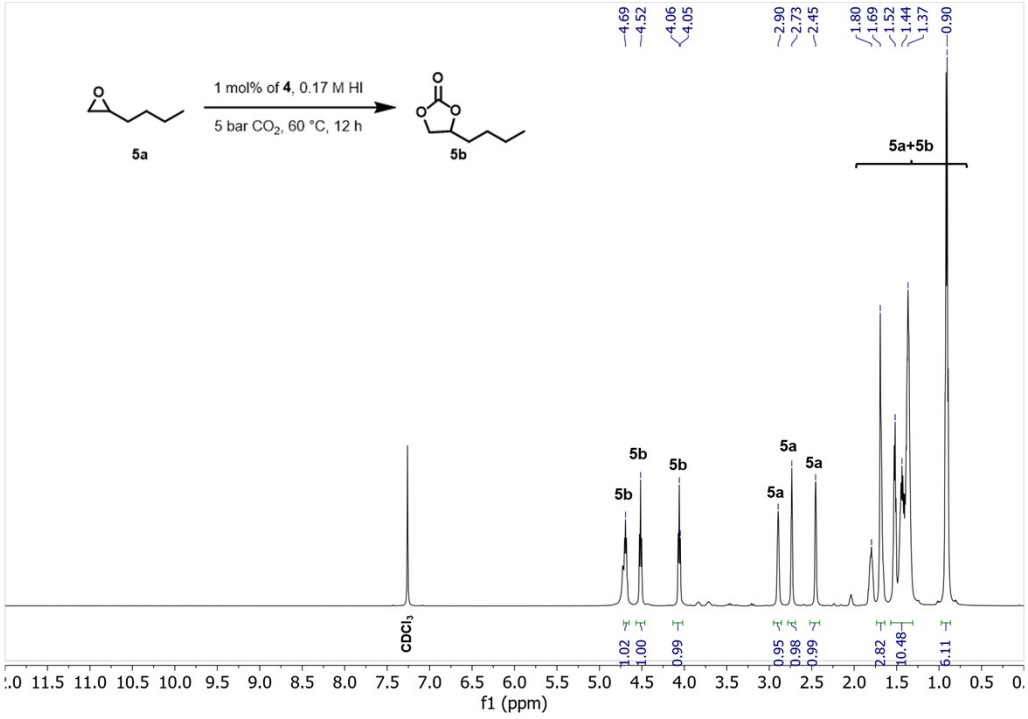

Figure S23. Crude ^{1}H NMR ($CDCl_3$) spectrum of cycloaddition of CO_2 to **5a** substrate by using 1 mol% of **4**, 0.5 mL of 0.17 M HI, 5 bar CO_2, 60 °C, 12 h; **Table 1, Entry 12**

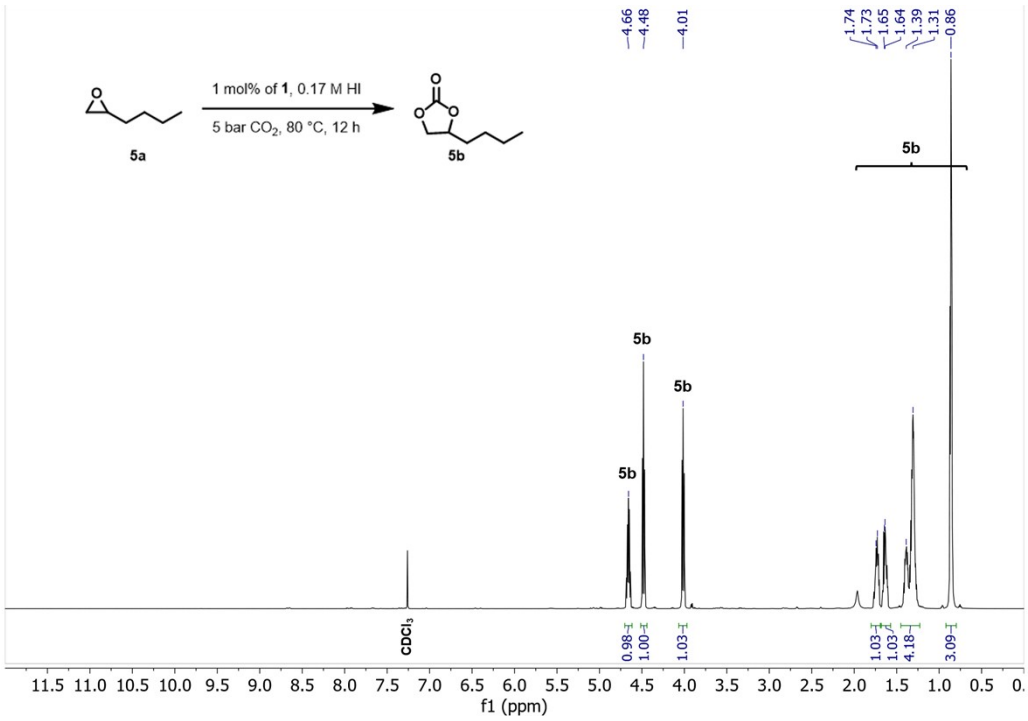

Figure S24. Crude ^{1}H NMR ($CDCl_3$) spectrum of cycloaddition of CO_2 to **5a** substrate by using 1 mol% of **1**, 0.5 mL of 0.17 M HI, 5 bar CO_2, 80 °C, 12 h; **Fig 2, Entry 1**

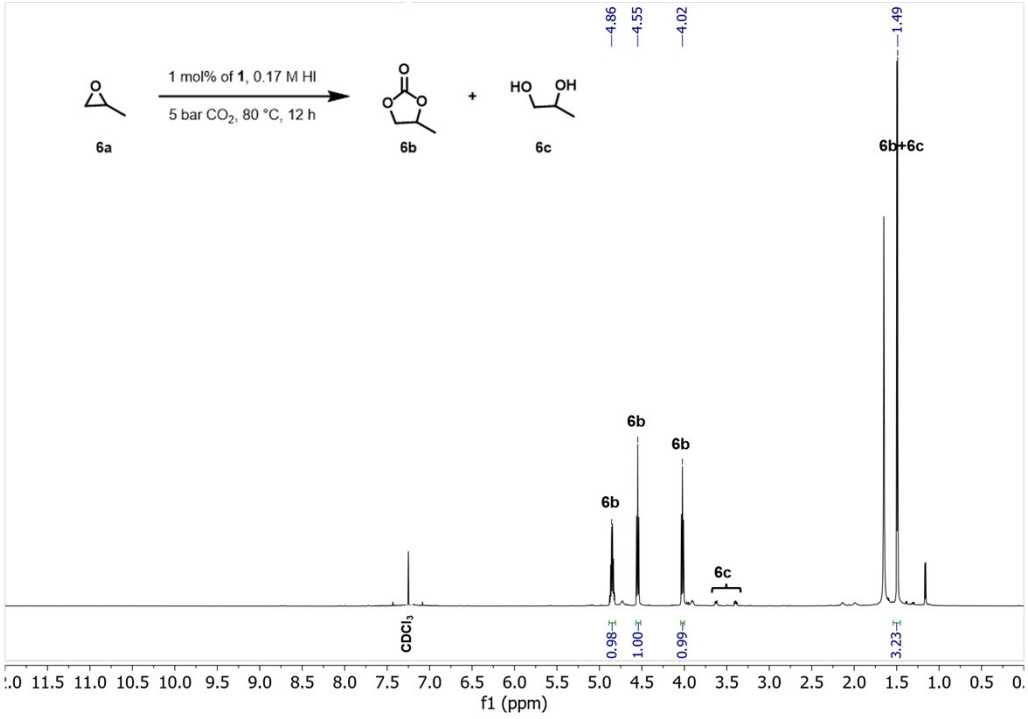

Figure S25. Crude ^{1}H NMR ($CDCl_3$) spectrum of cycloaddition of CO_2 to **6a** substrate by using 1 mol% of **1**, 0.5 mL of 0.17 M HI, 5 bar CO_2, 80 °C, 12 h; **Fig 2, Entry 2**

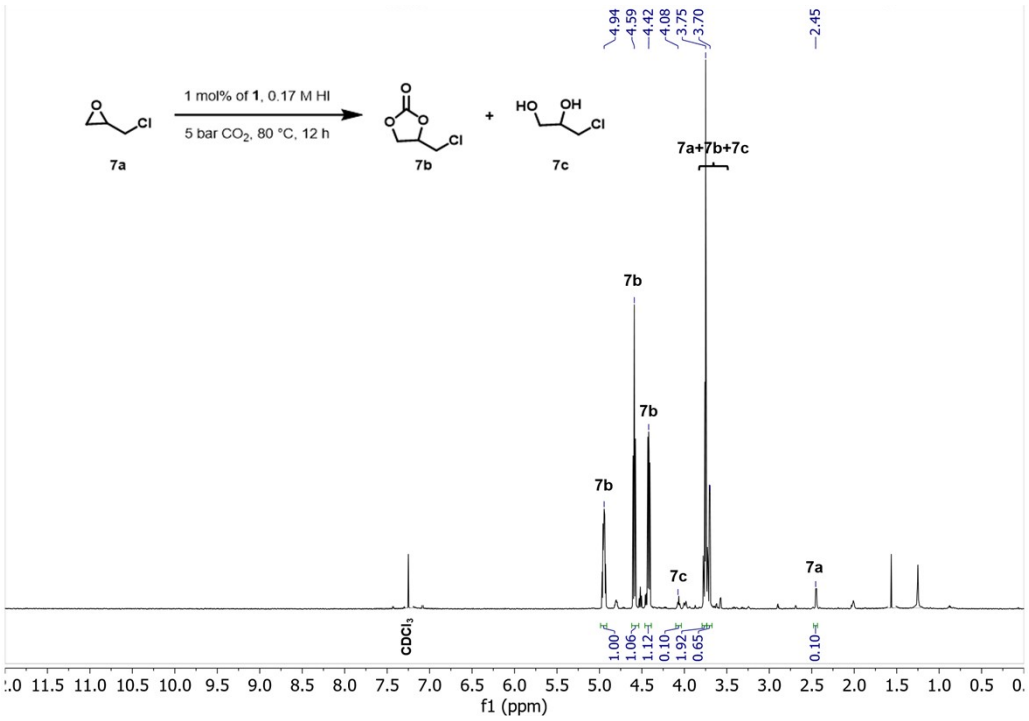

Figure S26. Crude ^{1}H NMR ($CDCl_3$) spectrum of cycloaddition of CO_2 to **7a** substrate by using 1 mol% of **1**, 0.5 mL of 0.17 M HI, 5 bar CO_2, 80 °C, 12 h; **Fig 2, Entry 3**

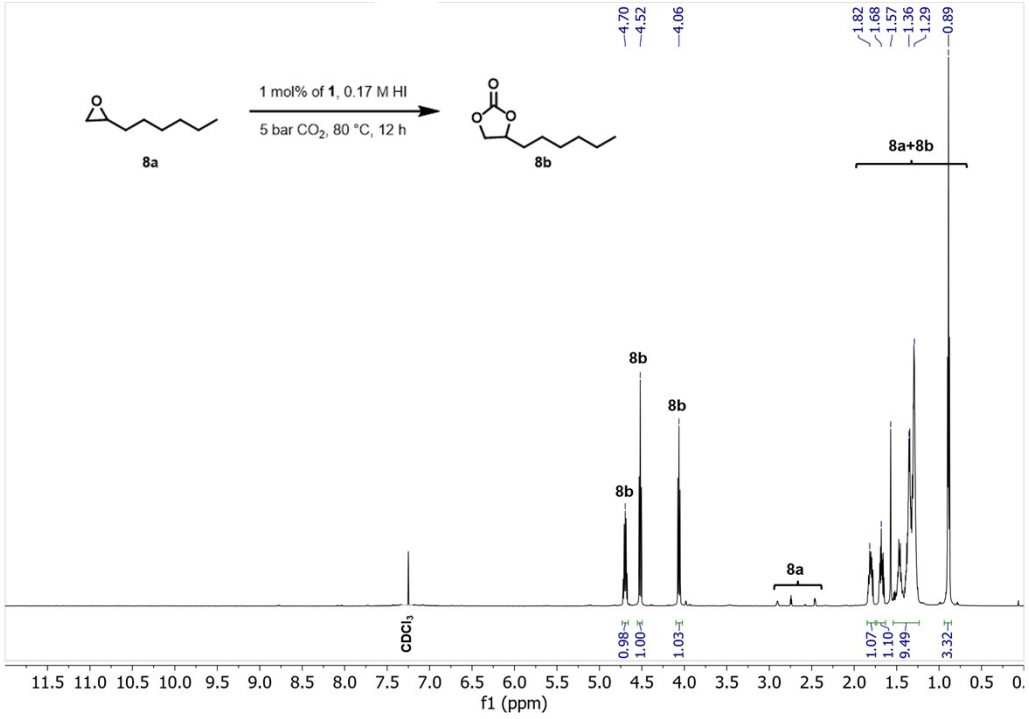

Figure S27. Crude ^{1}H NMR ($CDCl_3$) spectrum of cycloaddition of CO_2 to **8a** substrate by using 1 mol% of **1**, 0.5 mL of 0.17 M HI, 5 bar CO_2, 80 °C, 12 h; **Fig 2, Entry 4**

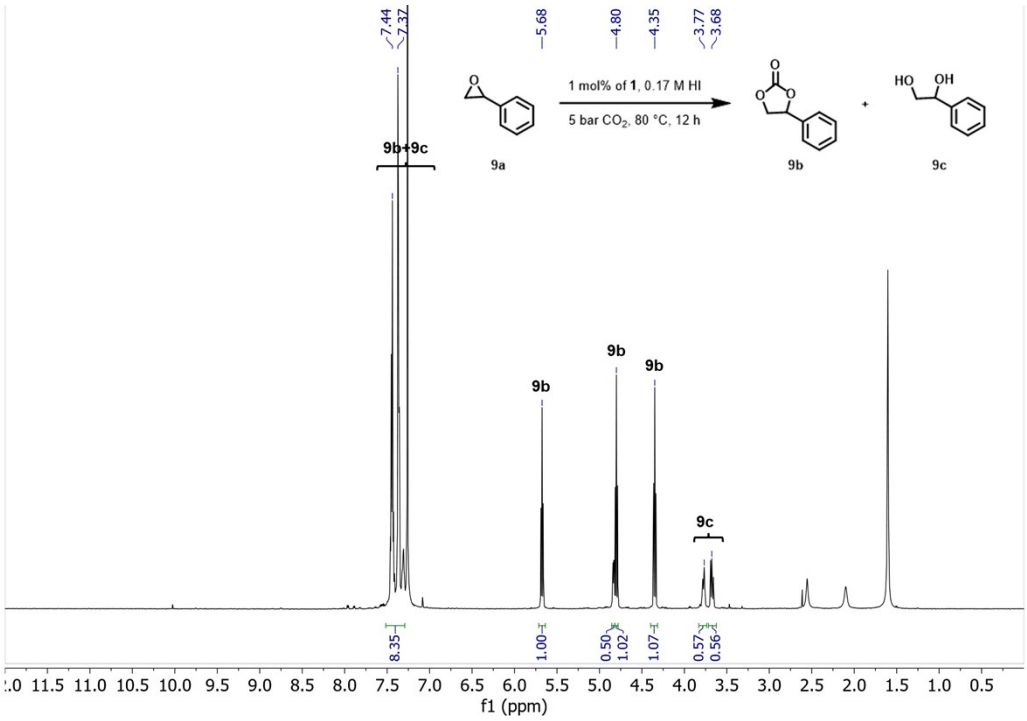

Figure S28. Crude ^{1}H NMR ($CDCl_3$) spectrum of cycloaddition of CO_2 to **9a** substrate by using 1 mol% of **1**, 0.5 mL of 0.17 M HI, 5 bar CO_2, 80 °C, 12 h; **Fig 2, Entry 5**

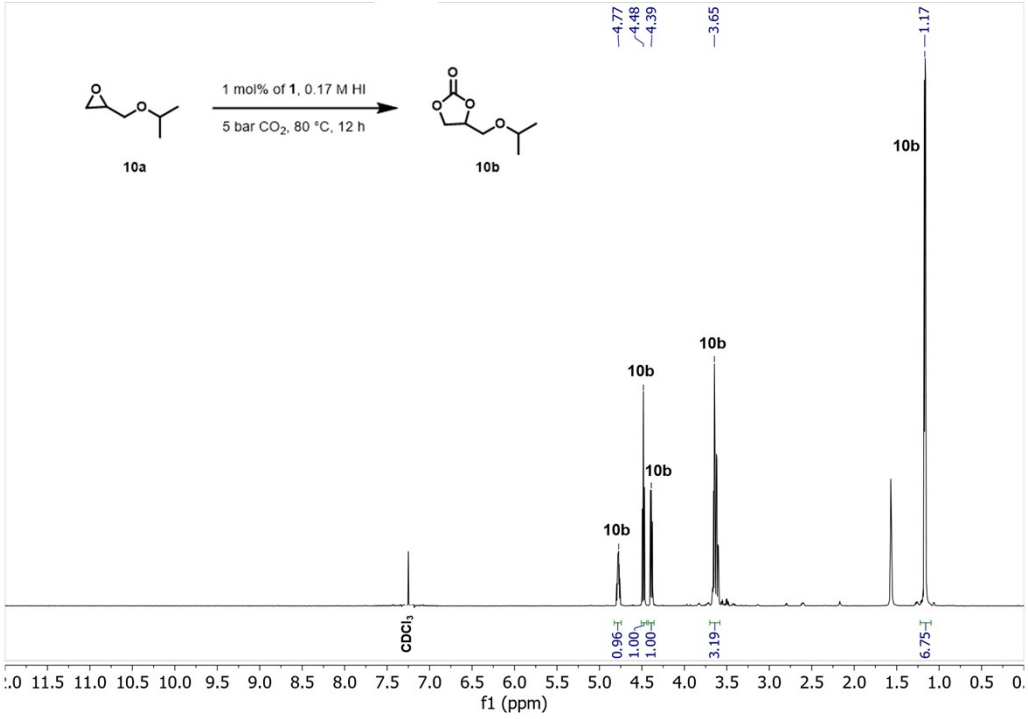

Figure S29. Crude ^{1}H NMR ($CDCl_3$) spectrum of cycloaddition of CO_2 to **10a** substrate by using 1 mol% of **1**, 0.5 mL of 0.17 M HI, 5 bar CO_2, 80 °C, 12 h; **Fig 2, Entry 6**

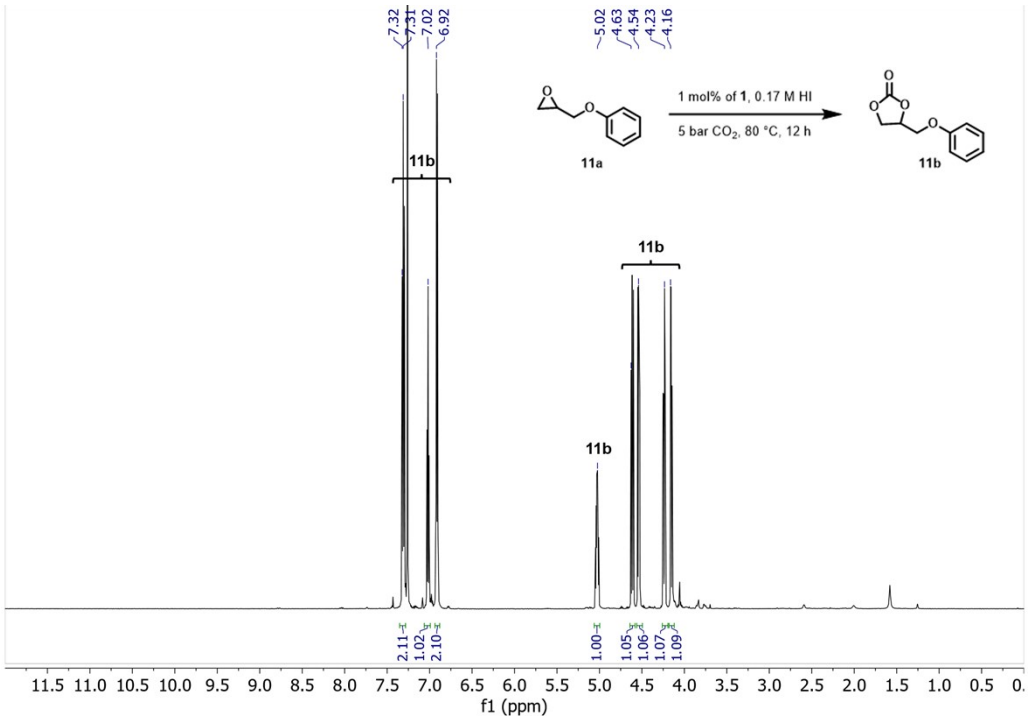

Figure S30. Crude ^{1}H NMR ($CDCl_3$) spectrum of cycloaddition of CO_2 to **11a** substrate by using 1 mol% of **1**, 0.5 mL of 0.17 M HI, 5 bar CO_2, 80 °C, 12 h; **Fig 2, Entry 7**

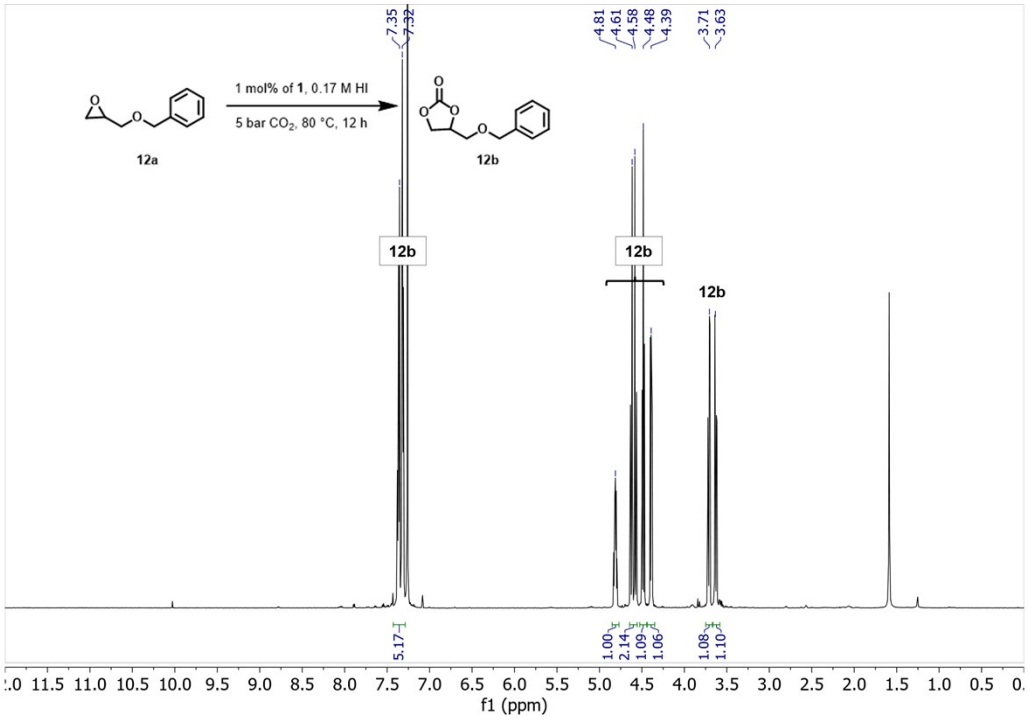

Figure S31. Crude ^{1}H NMR ($CDCl_3$) spectrum of cycloaddition of CO_2 to **12a** substrate by using 1 mol% of **1**, 0.5 mL of 0.17 M HI, 5 bar CO_2, 80 °C, 12 h; **Fig 2, Entry 8**

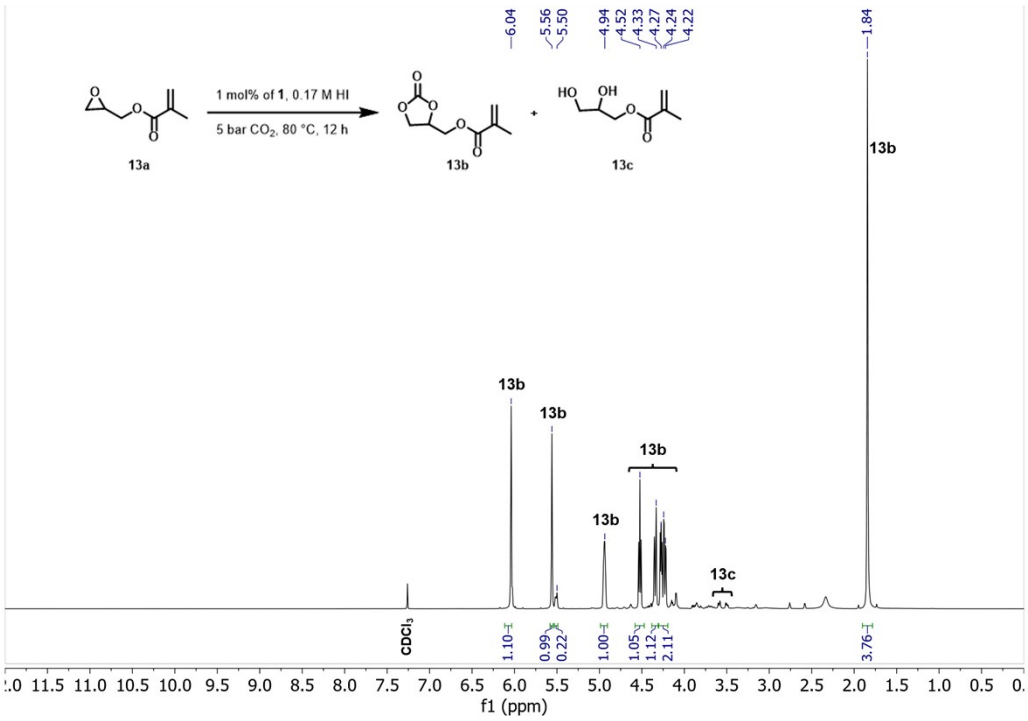

Figure S32. Crude ^{1}H NMR ($CDCl_3$) spectrum of cycloaddition of CO_2 to **13a** substrate by using 1 mol% of **1**, 0.5 mL of 0.17 M HI, 5 bar CO_2, 80 °C, 12 h; **Fig 2, Entry 9**

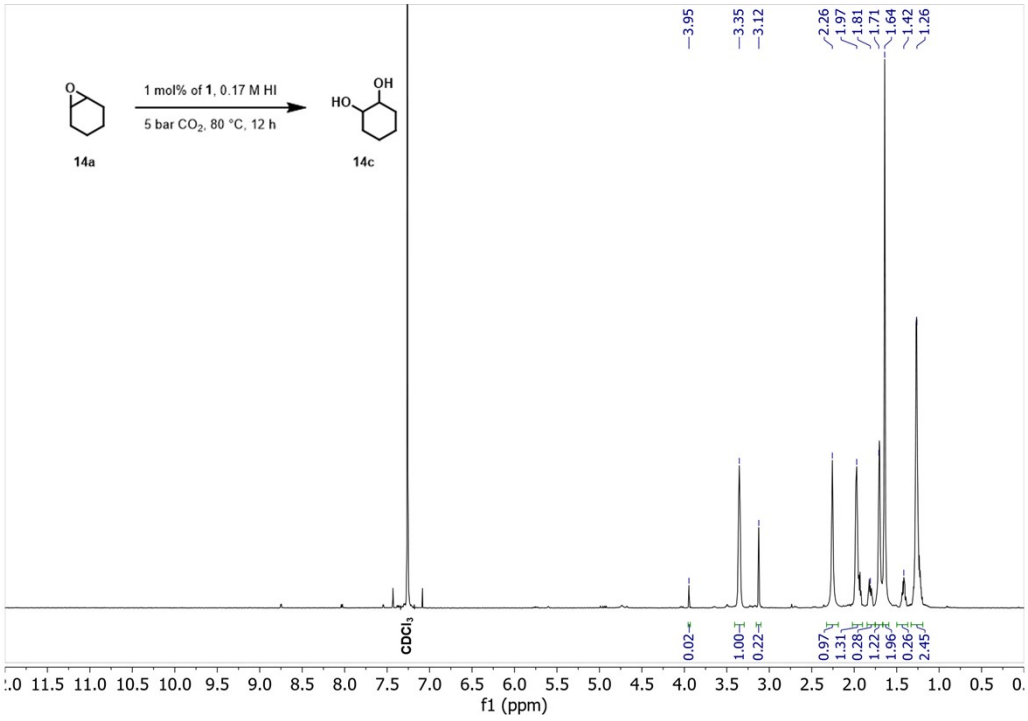

Figure S33. Crude ^{1}H NMR ($CDCl_3$) spectrum of cycloaddition of CO_2 to **14a** substrate by using 1 mol% of **1**, 0.5 mL of 0.17 M HI, 5 bar CO_2, 80 °C, 12 h; **Fig 2, Entry 10**

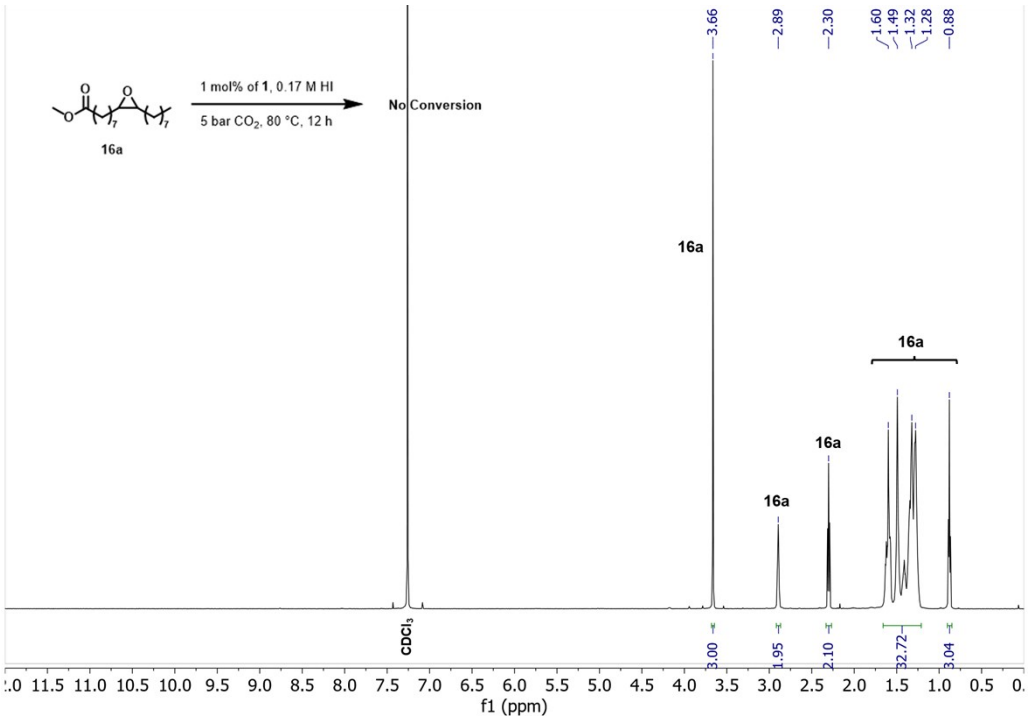

Figure S34. Crude ^{1}H NMR ($CDCl_3$) spectrum of cycloaddition of CO_2 to **16a** substrate by using 1 mol% of **1**, 0.5 mL of 0.17 M HI, 5 bar CO_2, 80 °C, 12 h; **Fig 2, Entry 11**

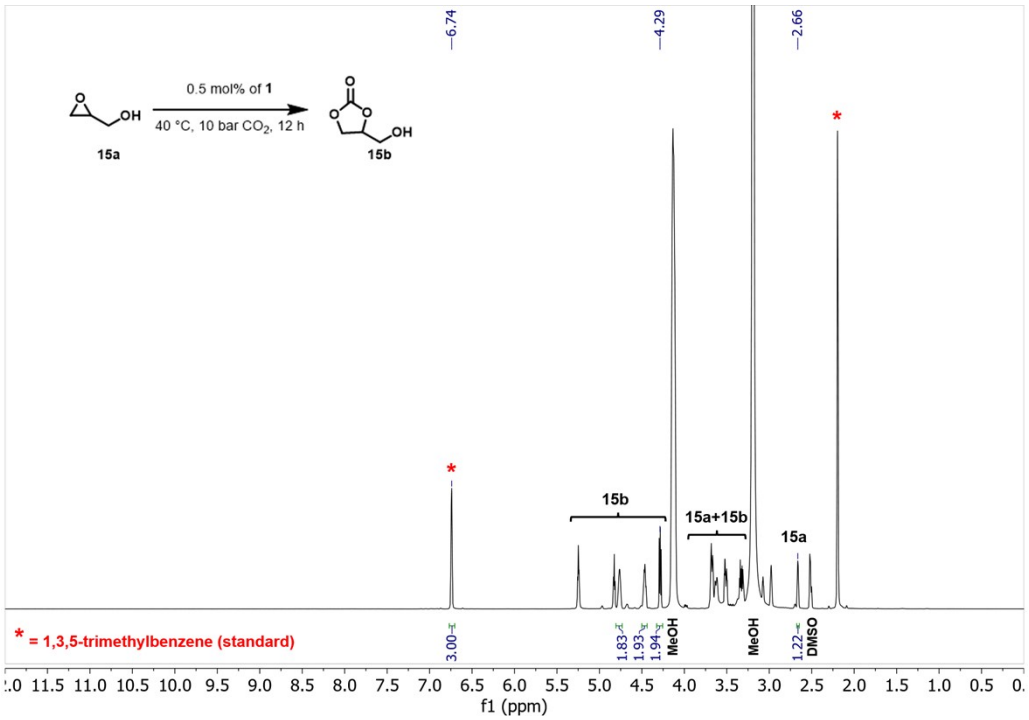

Figure S35. Crude ^{1}H NMR (DMSO-d_6) spectrum of cycloaddition of CO_2 to **15a** substrate by using 0.5 mol% of **1**, 10 bar CO_2, 40 °C, 12 h; **Table 2, Entry 1**

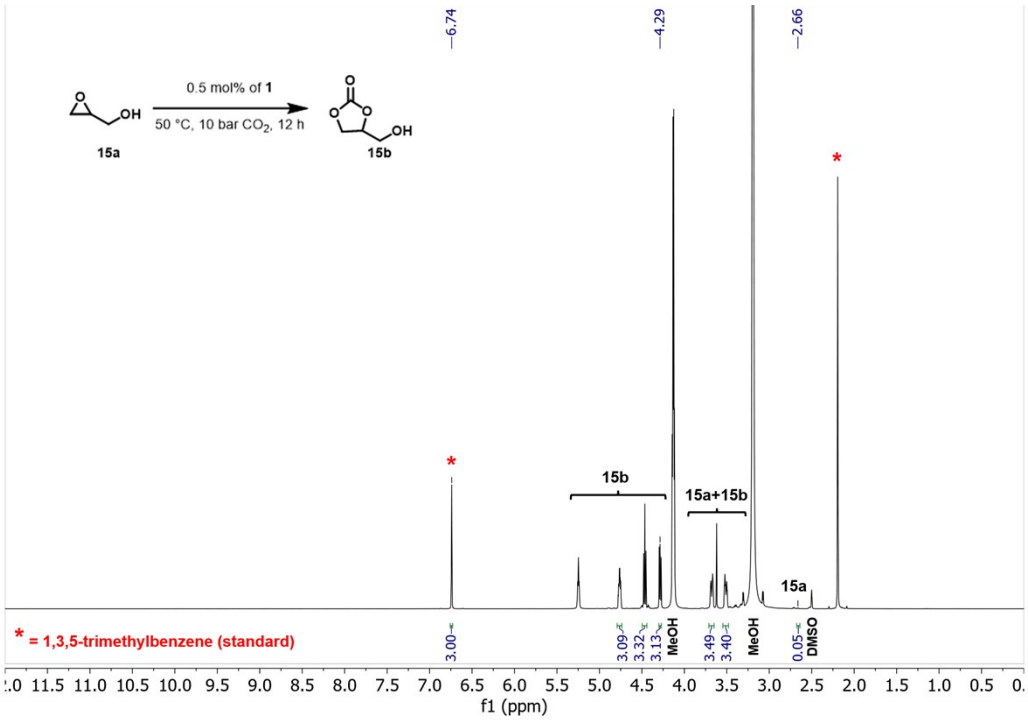

Figure S36. Crude ^{1}H NMR (DMSO-d_6) spectrum of cycloaddition of CO_2 to **15a** substrate by using 0.5 mol% of **1**, 10 bar CO_2, 50 °C, 12 h; **Table 2, Entry 2**

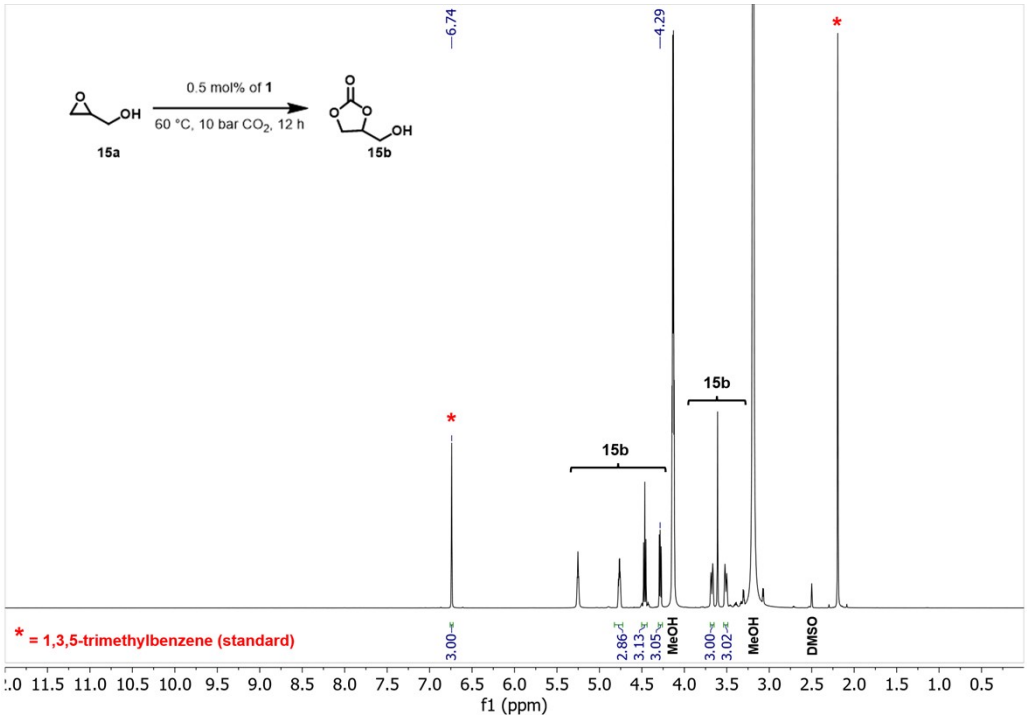

Figure S37. Crude ^{1}H NMR (DMSO-d_6) spectrum of cycloaddition of CO_2 to **15a** substrate by using 0.5 mol% of **1**, 10 bar CO_2, 60 °C, 12 h; **Table 2, Entry 3**

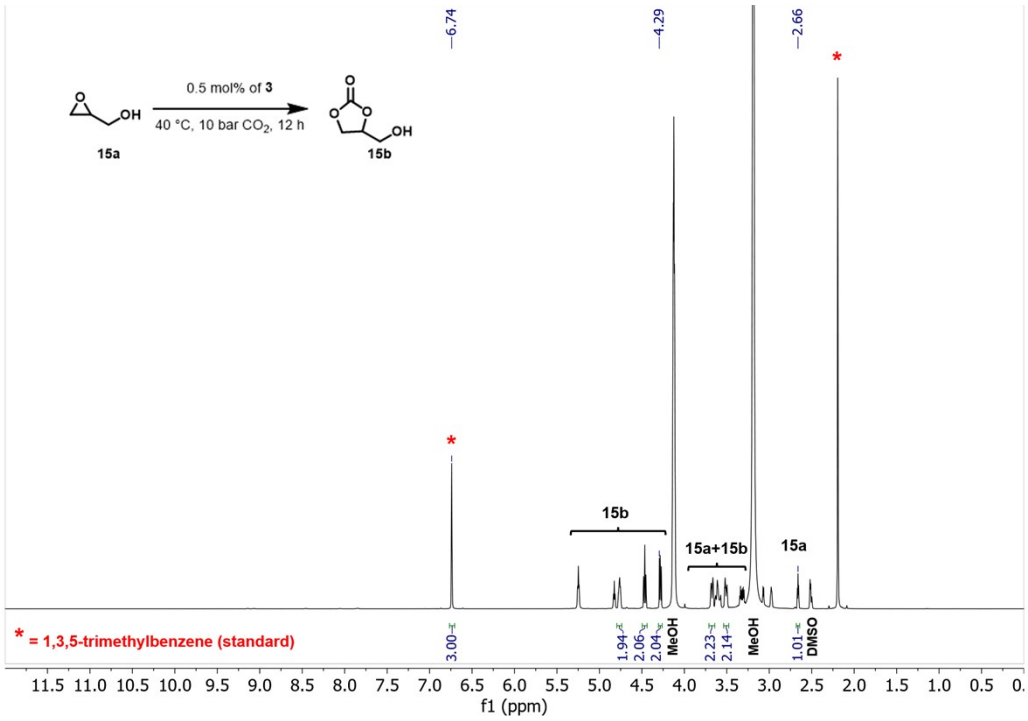

Figure S38. Crude ^{1}H NMR (DMSO-d_6) spectrum of cycloaddition of CO_2 to **15a** substrate by using 0.5 mol% of **3**, 10 bar CO_2, 40 °C, 12 h; **Table 2, Entry 4**

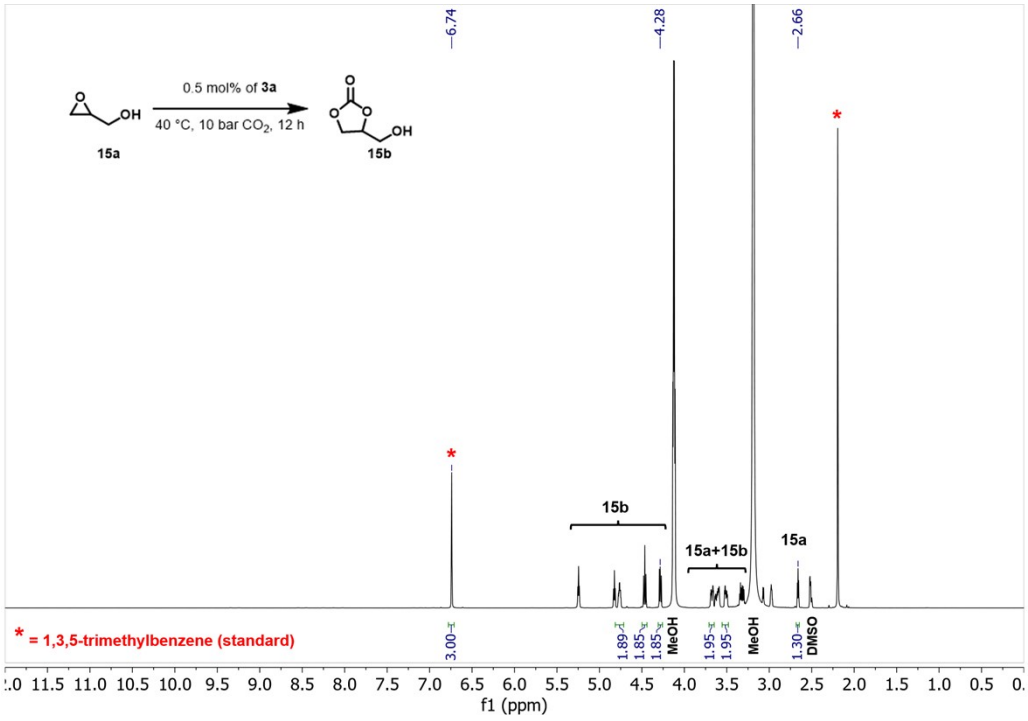

Figure S39. Crude ^{1}H NMR (DMSO-d_6) spectrum of cycloaddition of CO_2 to **15a** substrate by using 0.5 mol% of **3a**, 10 bar CO_2, 40 °C, 12 h; **Table 2, Entry 5**

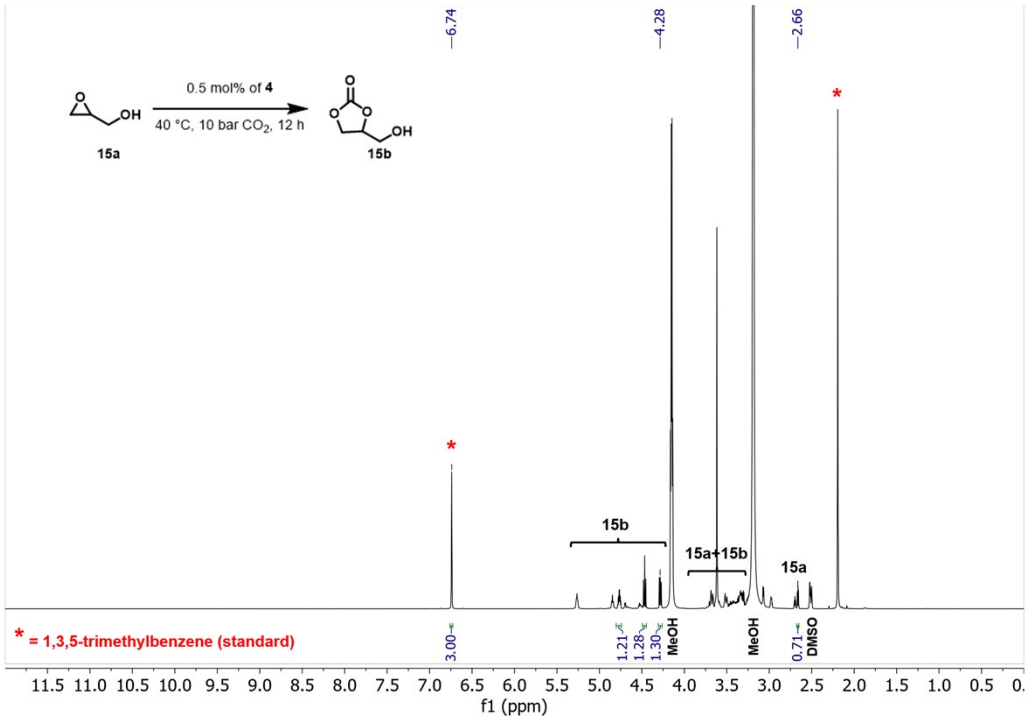

Figure S40. Crude ^{1}H NMR (DMSO-d_6) spectrum of cycloaddition of CO_2 to **15a** substrate by using 0.5 mol% of **4**, 10 bar CO_2, 40 °C, 12 h; **Table 2, Entry 6**

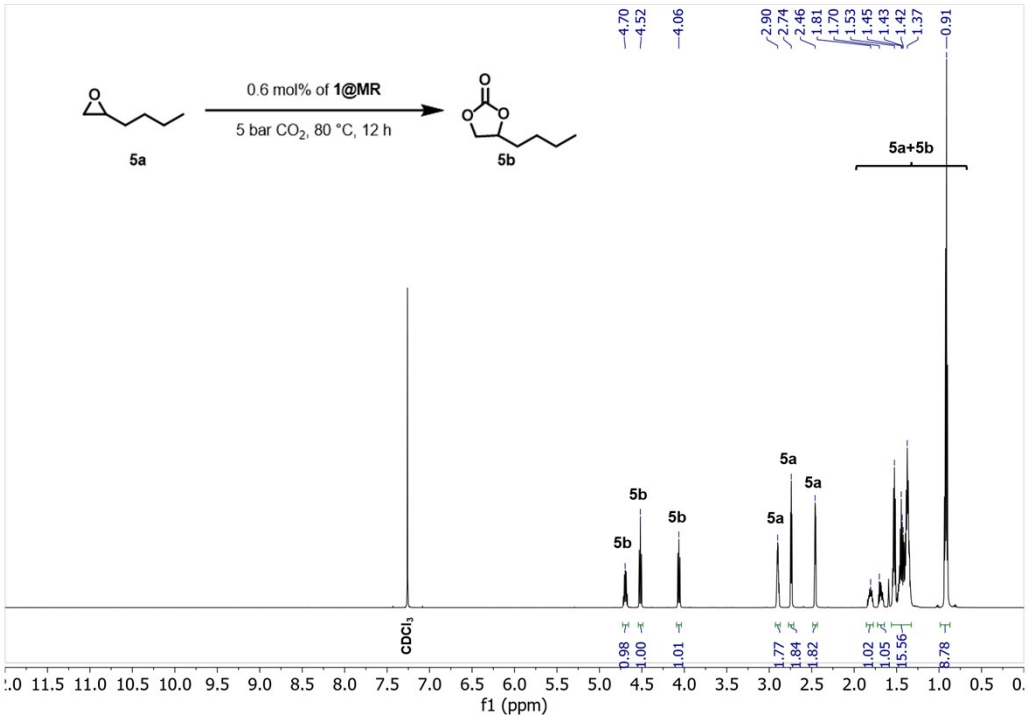

Figure S41. Crude ^{1}H NMR ($CDCl_3$) spectrum of cycloaddition of CO_2 to **5a** substrate by using 0.6 mol% of **1@MR**, 5 bar CO_2, 80 °C, 12 h; **Table 3, Entry 1**

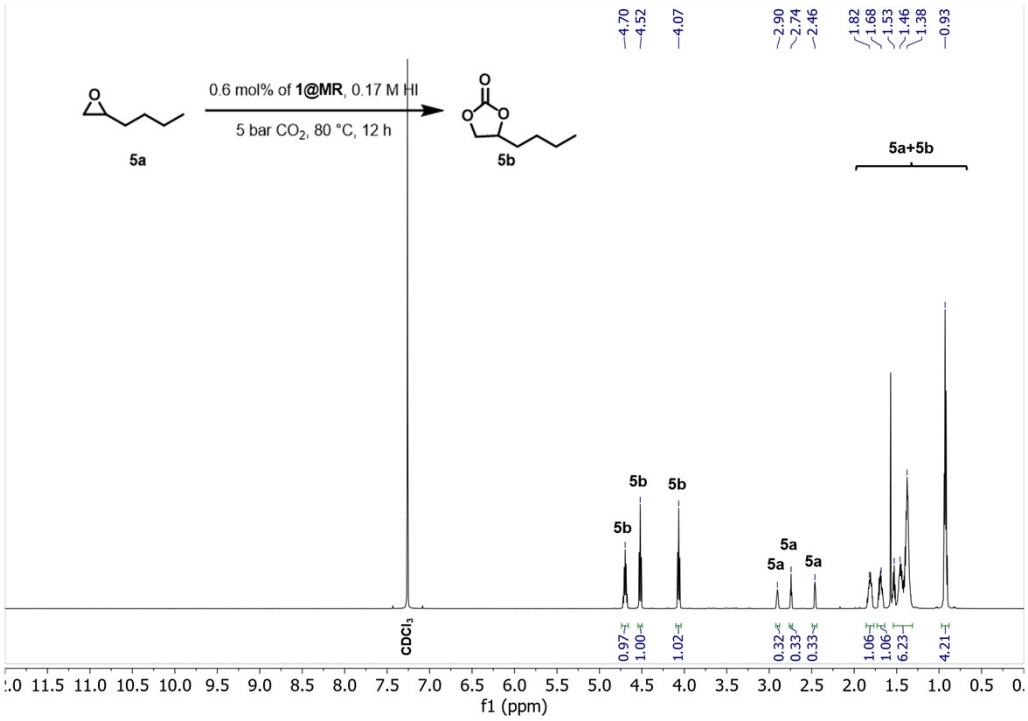

Figure S42. Crude ^{1}H NMR ($CDCl_3$) spectrum of cycloaddition of CO_2 to **5a** substrate by using 0.6 mol% of **1@MR**, 0.5 mL of 0.17 M HI, 5 bar CO_2, 80 °C, 12 h; **Table 3, Entry 2**

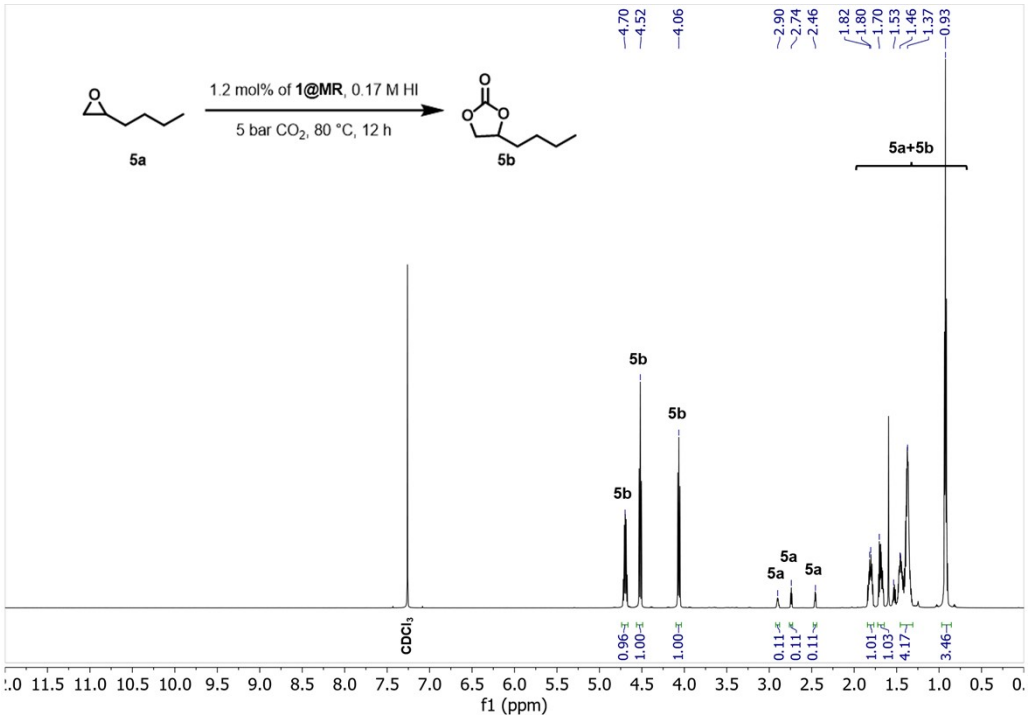

Figure S43. Crude ^{1}H NMR ($CDCl_3$) spectrum of cycloaddition of CO_2 to **5a** substrate by using 1.2 mol% of **1@MR**, 0.5 mL of 0.17 M HI, 5 bar CO_2, 80 °C, 12 h; **Table 3, Entry 3**

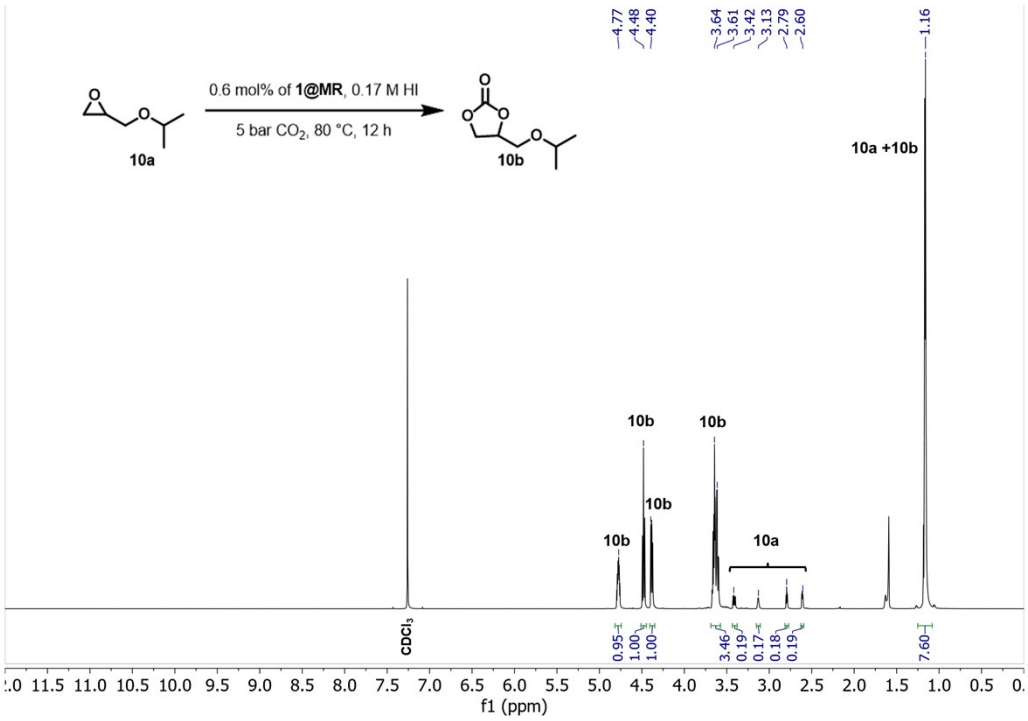

Figure S44. Crude ^{1}H NMR ($CDCl_3$) spectrum of cycloaddition of CO_2 to **10a** substrate by using 0.6 mol% of **1@MR**, 0.5 mL of 0.17 M HI, 5 bar CO_2, 80 °C, 12 h; **Table 3, Entry 4**

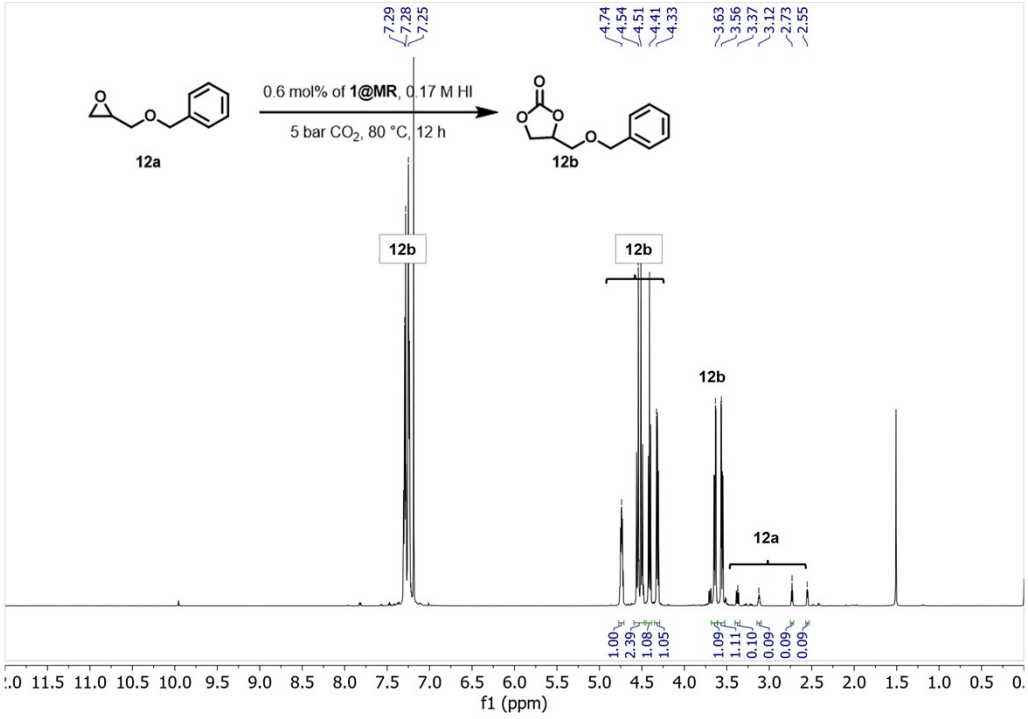

Figure S45. Crude ^{1}H NMR ($CDCl_3$) spectrum of cycloaddition of CO_2 to **12a** substrate by using 0.6 mol% of **1@MR**, 0.5 mL of 0.17 M HI, 5 bar CO_2, 80 °C, 12 h; **Table 3, Entry 5**

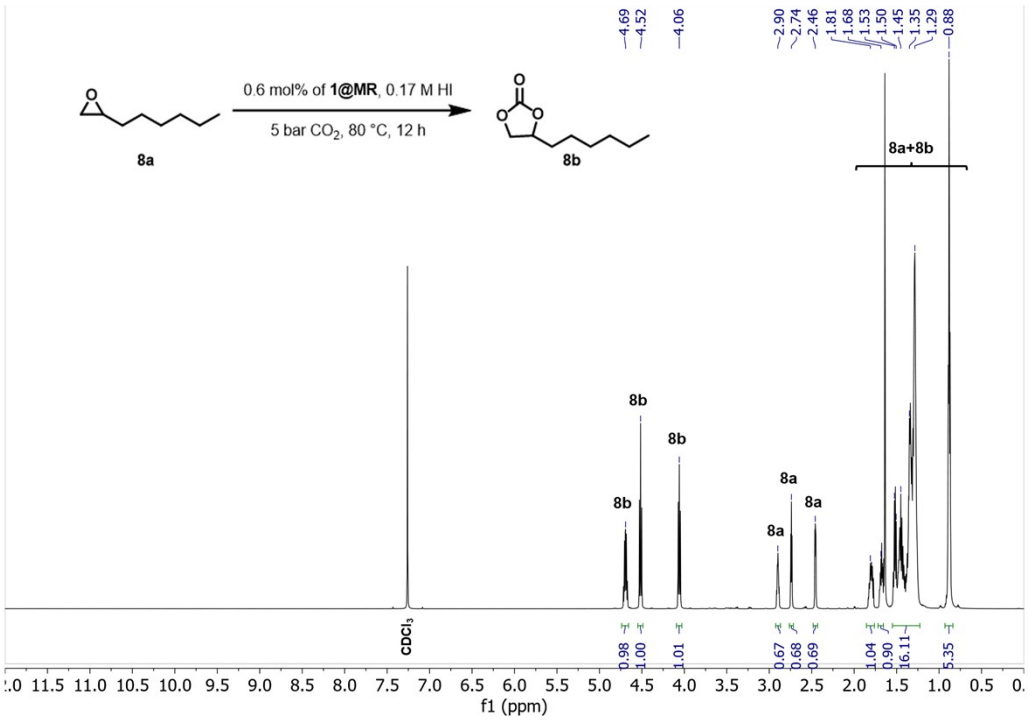

Figure S46. Crude ^{1}H NMR ($CDCl_3$) spectrum of cycloaddition of CO_2 to **8a** substrate by using 0.6 mol% of **1@MR**, 0.5 mL of 0.17 M HI, 5 bar CO_2, 80 °C, 12 h; **Table 3, Entry 6**

Isolated compound spectra

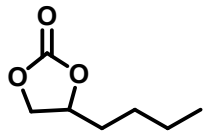

4-butyl-1,3-dioxolan-2-one (**5b**). Colorless liquid. ^{1}H NMR (600 MHz, Chloroform-*d*) δ 4.66 (dd, *J* = 7.6, 5.4 Hz, 1H), 4.48 (t, *J* = 8.2 Hz, 1H), 4.01 (dd, *J* = 8.5, 7.2 Hz, 1H), 1.74 (d, *J* = 3.4 Hz, 1H), 1.64 (dd, *J* = 9.5, 4.6 Hz, 1H), 1.42 – 1.22 (m, 4H), 0.86 (t, *J* = 7.1 Hz, 3H).
^{13}C NMR (151 MHz, Chloroform-*d*) δ 155.21, 77.17, 69.46, 33.46, 26.39, 22.20, 13.74.

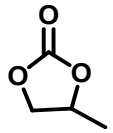

4-methyl-1,3-dioxolan-2-one (**6b**). Colorless liquid. ^{1}H NMR (600 MHz, Chloroform-*d*) δ 4.88 – 4.77 (m, 1H), 4.53 (dd, *J* = 8.5, 7.7 Hz, 1H), 4.00 (dd, *J* = 8.5, 7.2 Hz, 1H), 1.45 (d, *J* = 6.3 Hz, 3H).
^{13}C NMR (151 MHz, Chloroform-*d*) δ 155.12, 73.63, 70.70, 19.39.

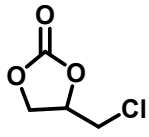

4-(chloromethyl)-1,3-dioxolan-2-one (**7b**). Colorless liquid. ^{1}H NMR (600 MHz, Chloroform-*d*) δ 5.01 – 4.93 (m, 1H), 4.60 – 4.52 (m, 1H), 4.37 (dd, *J* = 8.9, 5.7 Hz, 1H), 3.79 (dd, *J* = 12.3, 4.9 Hz, 1H), 3.70 (dd, *J* = 12.3, 3.7 Hz, 1H).
13C NMR (151 MHz, Chloroform-d) δ 154.50, 74.50, 67.00, 44.05.

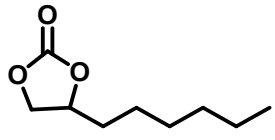

4-hexyl-1,3-dioxolan-2-one (**8b**). Colorless liquid. ^{1}H NMR (600 MHz, Chloroform-*d*) δ 4.64 (dd, *J* = 7.5, 5.3 Hz, 1H), 4.46 (s, 1H), 3.99 (d, *J* = 1.4 Hz, 1H), 1.70 (d, *J* = 3.0 Hz, 1H), 1.64 – 1.56 (m, 1H), 1.43 – 1.33 (m, 1H), 1.24 (dd, *J* = 33.7, 4.9 Hz, 7H), 0.80 (t, *J* = 7.0 Hz, 3H).
^{13}C NMR (151 MHz, Chloroform-*d*) δ 155.17, 77.16, 69.43, 33.74, 31.45, 28.72, 24.26, 22.39, 13.90.

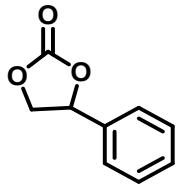

4-phenyl-1,3-dioxolan-2-one (**9b**). Colorless liquid. ^{1}H NMR (600 MHz, Chloroform-*d*) δ 7.44 – 7.37 (m, 3H), 7.36 – 7.31 (m, 2H), 5.66 (t, *J* = 8.0 Hz, 1H), 4.78 (t, *J* = 8.4 Hz, 1H), 4.35 – 4.25 (m, 1H).
^{13}C NMR (151 MHz, Chloroform-*d*) δ 155.00, 135.90, 129.72, 129.23, 125.98, 78.08, 71.23.

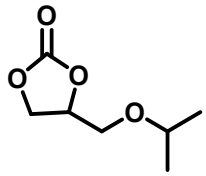

4-(isopropoxymethyl)-1,3-dioxolan-2-one (**10b**). Colorless liquid. ^{1}H NMR (600 MHz, Chloroform-*d*) δ 4.74 (dd, *J* = 8.4, 5.9 Hz, 1H), 4.42 (t, *J* = 8.4 Hz, 1H), 4.32 – 4.26 (m, 1H), 3.62 – 3.48 (m, 3H), 1.08 (d, *J* = 6.4 Hz, 6H).
^{13}C NMR (151 MHz, Chloroform-*d*) δ 155.22, 75.40, 72.77, 67.10, 66.35, 21.83, 21.72.

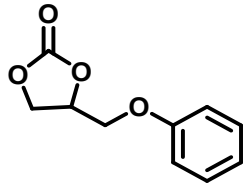

4-(phenoxymethyl)-1,3-dioxolan-2-one (**11b**). White solid. ^{1}H NMR (600 MHz, Chloroform-*d*) δ 7.34 – 7.28 (m, 2H), 7.02 (t, *J* = 7.3 Hz, 1H), 6.91 (d, *J* = 7.7 Hz, 2H), 5.02 (dd, *J* = 4.1, 1.6 Hz, 1H), 4.61 (t, *J* = 8.5 Hz, 1H), 4.55 – 4.51 (m, 1H), 4.23 (dd, *J* = 10.6, 4.2 Hz, 1H), 4.14 (dd, *J* = 10.6, 3.6 Hz, 1H).
^{13}C NMR (151 MHz, Chloroform-*d*) δ 157.79, 154.68, 129.72, 122.03, 114.65, 77.26, 74.14, 66.92, 66.26.

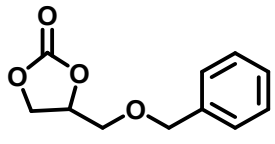

4-((benzyloxy)methyl)-1,3-dioxolan-2-one (**12b**). Colorless liquid. ^{1}H NMR (600 MHz, Chloroform-*d*) δ 7.40 – 7.24 (m, 5H), 4.77 (d, *J* = 2.5 Hz, 1H), 4.55 (d, *J* = 12.3 Hz, 2H), 4.41 (s, 1H), 4.32 (d, *J* = 5.9 Hz, 1H), 3.67 (dd, *J* = 11.2, 3.4 Hz, 1H), 3.56 (dd, *J* = 11.2, 3.7 Hz, 1H).
^{13}C NMR (151 MHz, Chloroform-*d*) δ 155.24, 137.40, 128.58, 128.02, 127.73, 75.33, 73.54, 69.02, 66.30.

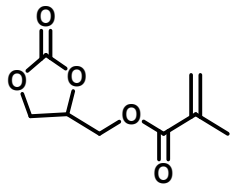

(2-oxo-1,3-dioxolan-4-yl)methyl methacrylate (**13b**). Colorless liquid. ^{1}H NMR (600 MHz, Chloroform-*d*) δ 6.08 (s, 1H), 5.59 (s, 1H), 4.96 (d, *J* = 3.5 Hz, 1H), 4.55 (s, 1H), 4.42 – 4.34 (m, 1H), 4.32 – 4.23 (m, 2H), 1.93 – 1.85 (m, 3H).
^{13}C NMR (151 MHz, Chloroform-*d*) δ 166.60, 154.67, 135.20, 127.11, 73.99, 66.17, 63.48, 18.08.

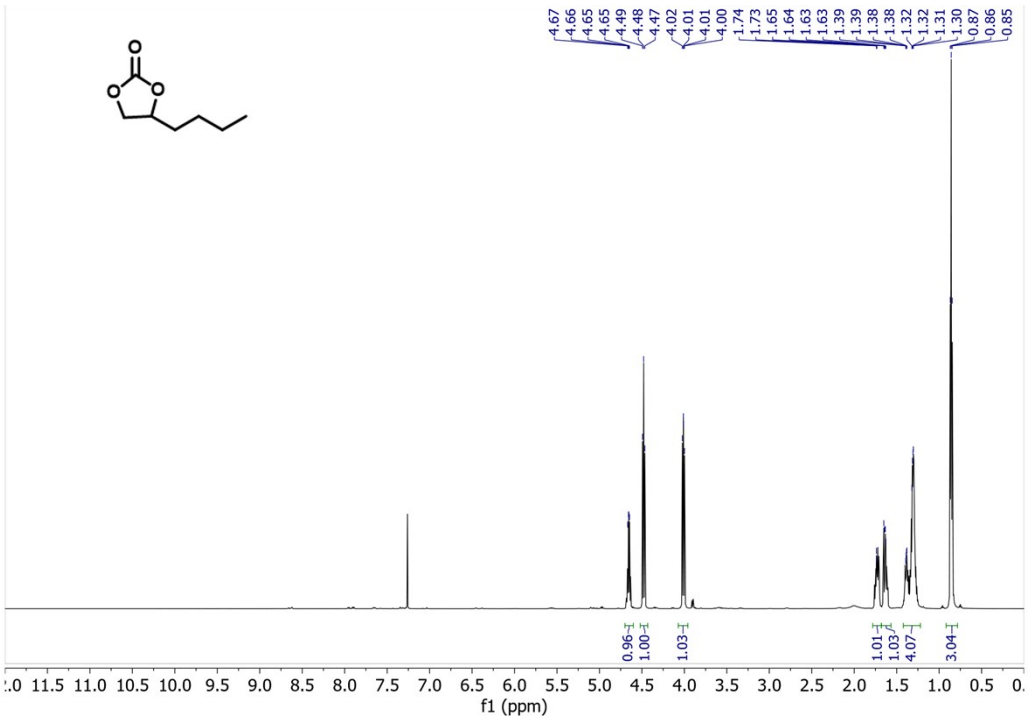

Figure S47. ^{1}H NMR ($CDCl_3$) spectrum of **5b** after chromatographic purification.

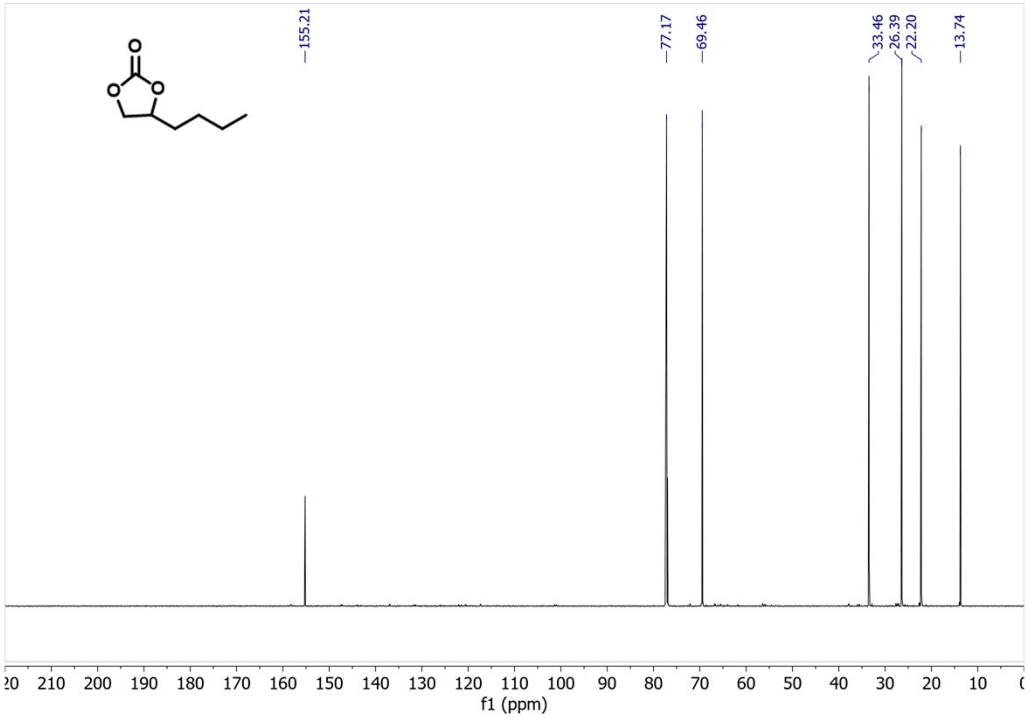

Figure S48. ^{13}C NMR ($CDCl_3$) spectrum of **5b** after chromatographic purification.

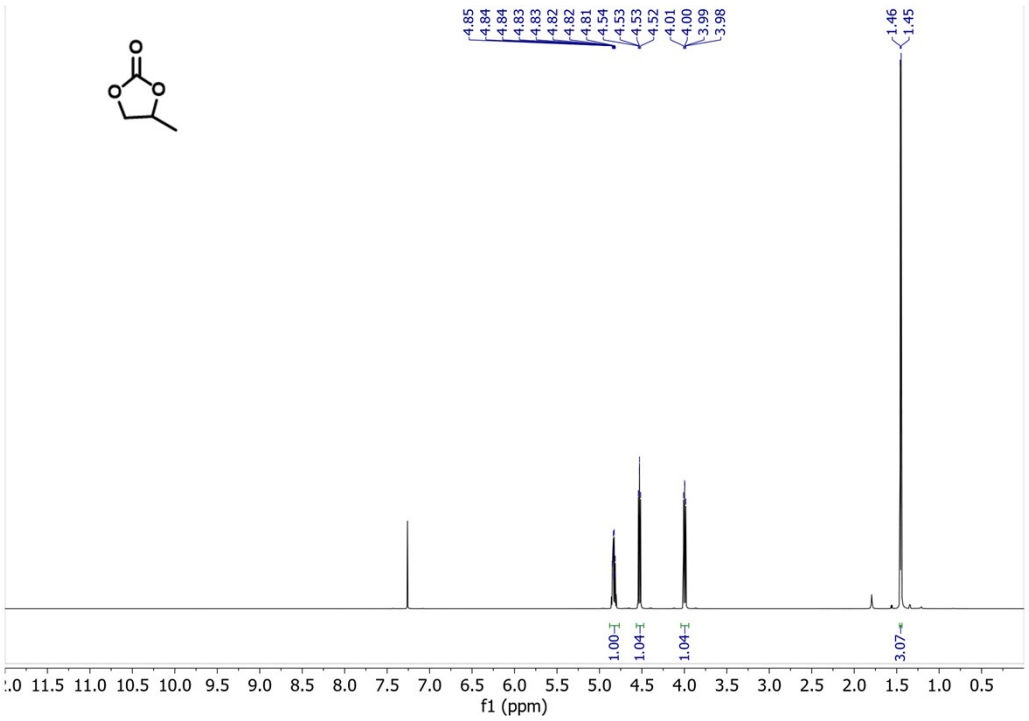

Figure S49. ^{1}H NMR ($CDCl_3$) spectrum of **6b** after chromatographic purification.

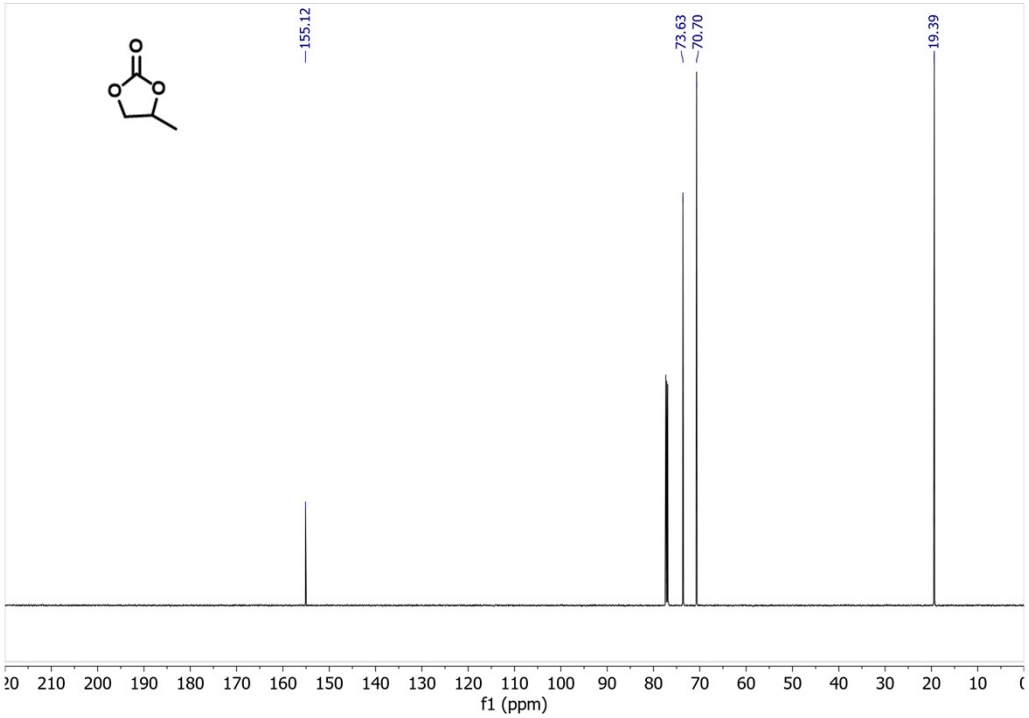

Figure S50. ^{13}C NMR ($CDCl_3$) spectrum of **6b** after chromatographic purification.

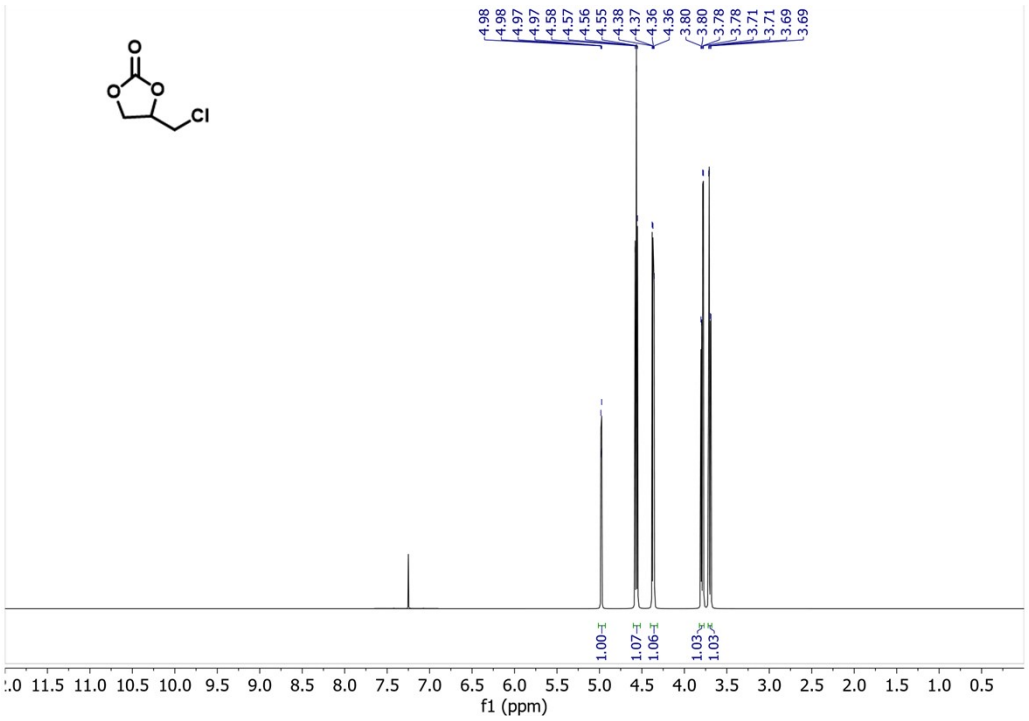

Figure S51. ^{1}H NMR ($CDCl_3$) spectrum of **7b** after chromatographic purification.

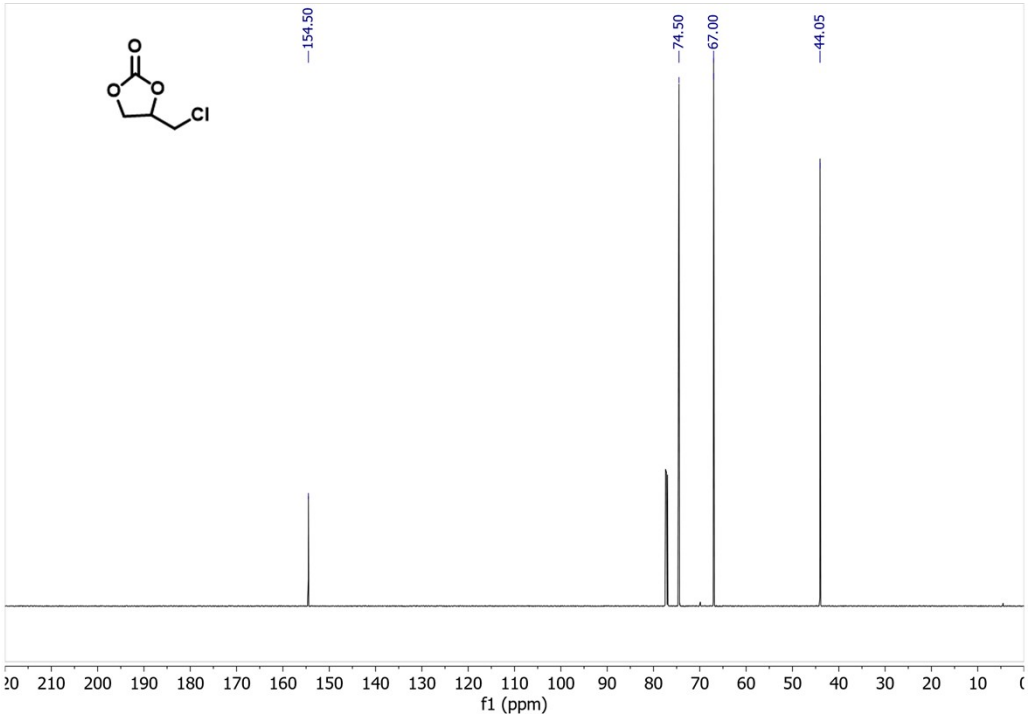

Figure S52. ^{13}C NMR ($CDCl_3$) spectrum of **7b** after chromatographic purification.

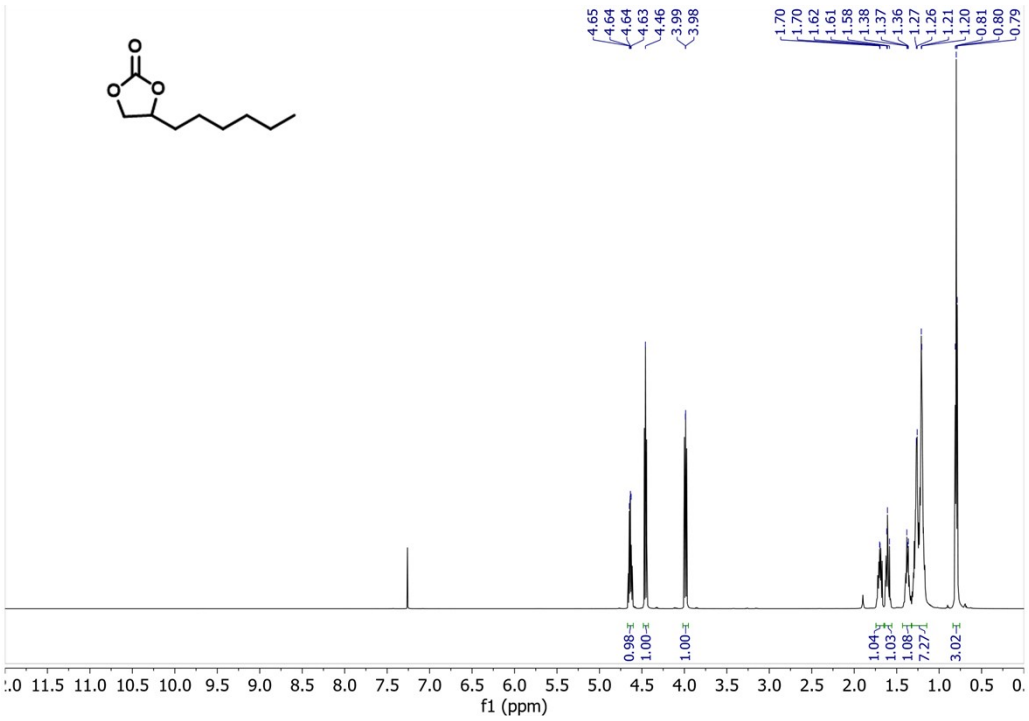

Figure S53. ^{1}H NMR ($CDCl_3$) spectrum of **8b** after chromatographic purification.

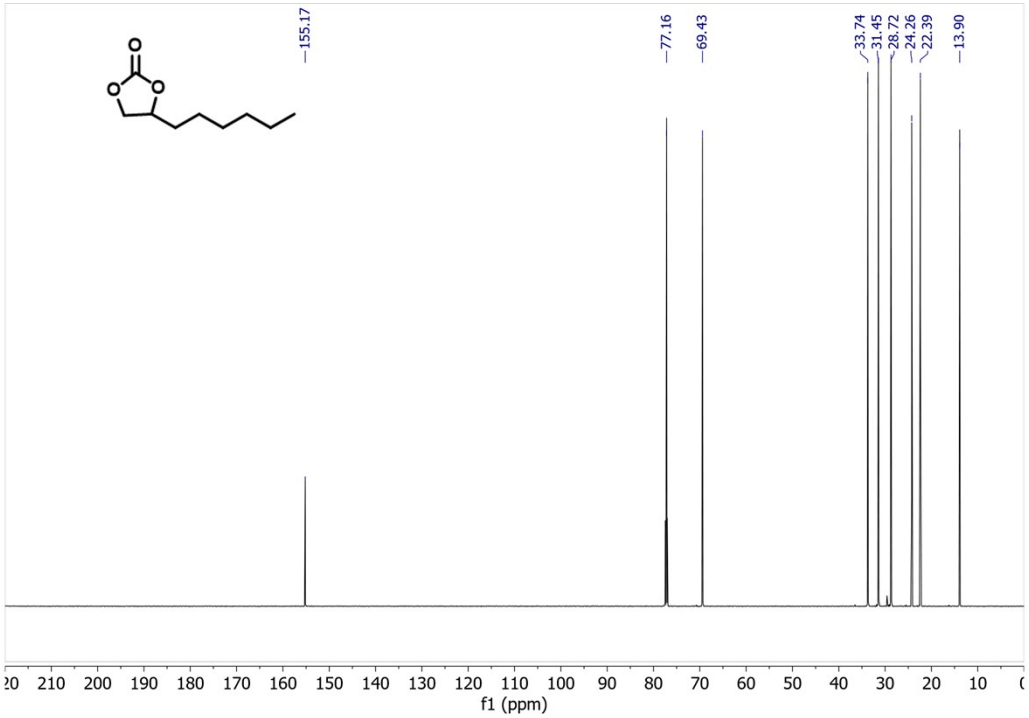

Figure S54. ^{13}C NMR ($CDCl_3$) spectrum of **8b** after chromatographic purification.

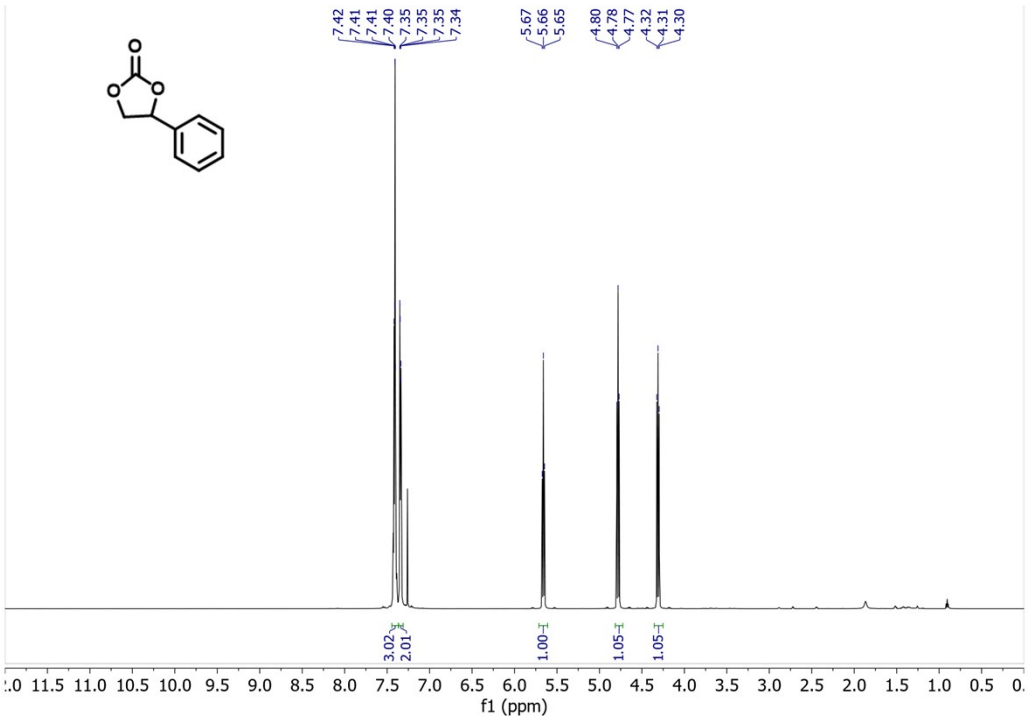

Figure S55. ^{1}H NMR ($CDCl_3$) spectrum of **9b** after chromatographic purification.

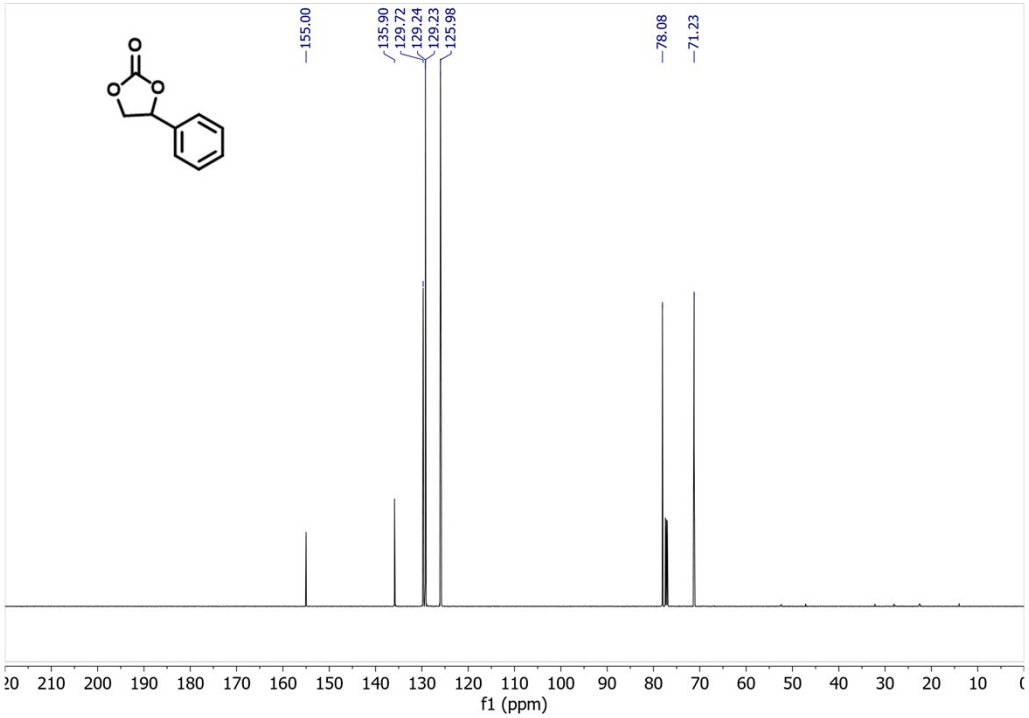

Figure S56. ^{13}C NMR ($CDCl_3$) spectrum of **9b** after chromatographic purification.

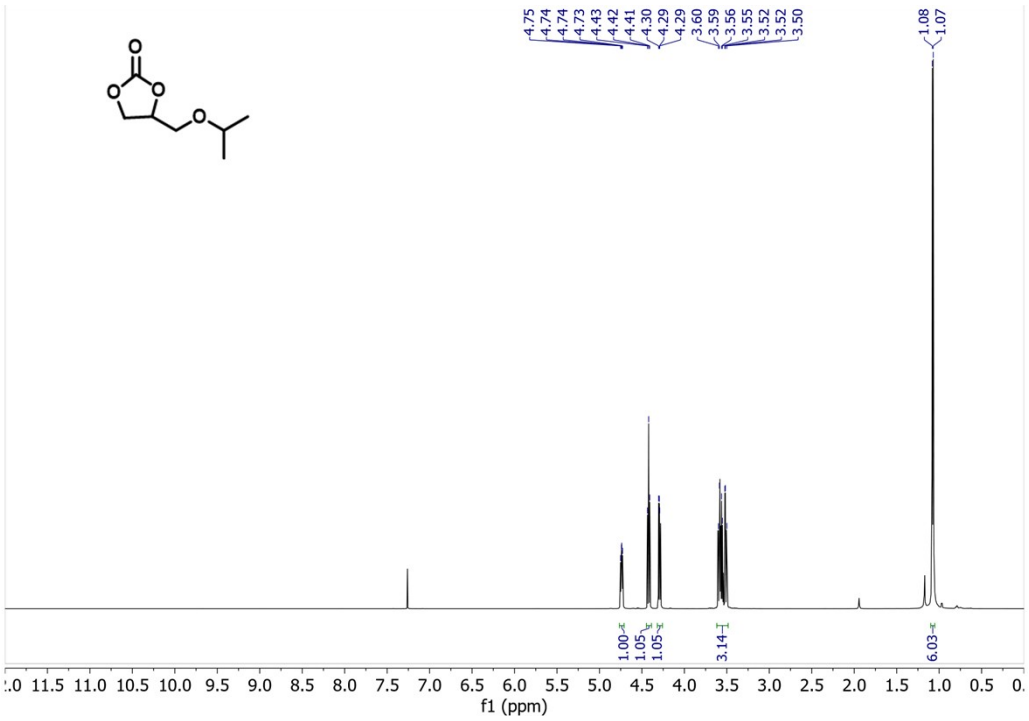

Figure S57. ^{1}H NMR ($CDCl_3$) spectrum of **10b** after chromatographic purification.

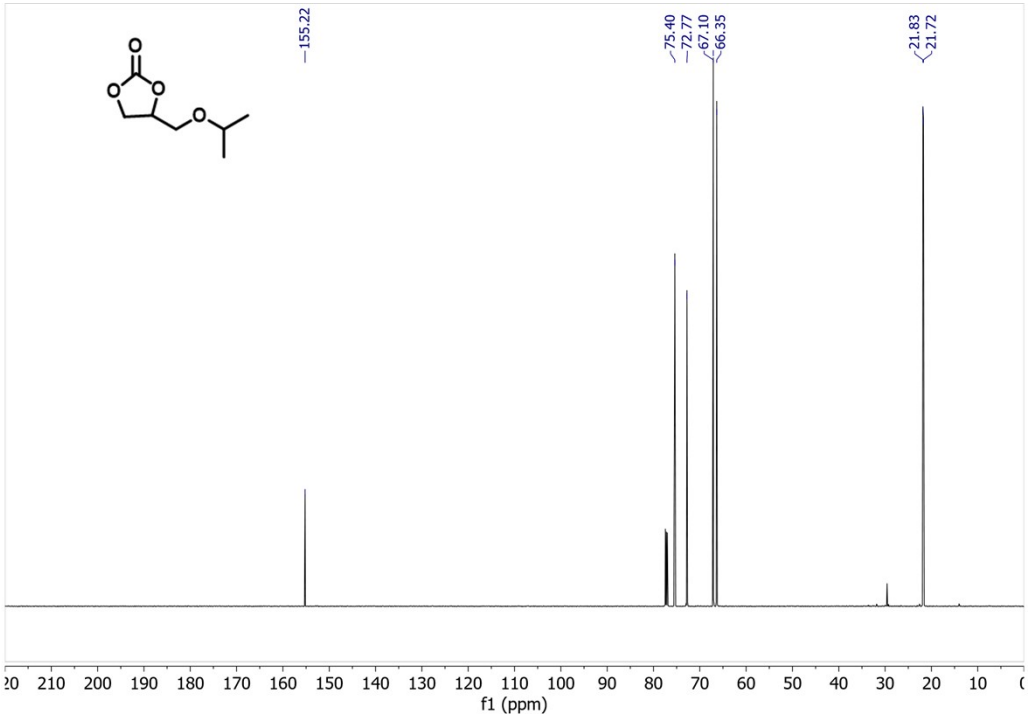

Figure S58. ^{13}C NMR ($CDCl_3$) spectrum of **10b** after chromatographic purification.

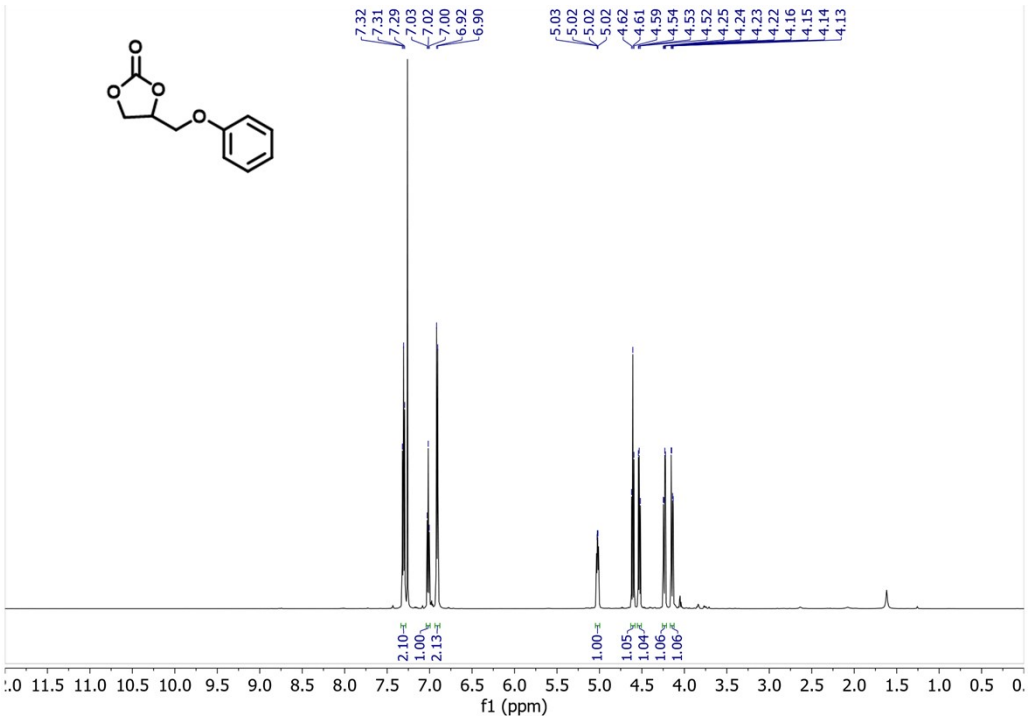

Figure S59. ^{1}H NMR ($CDCl_3$) spectrum of **11b** after chromatographic purification.

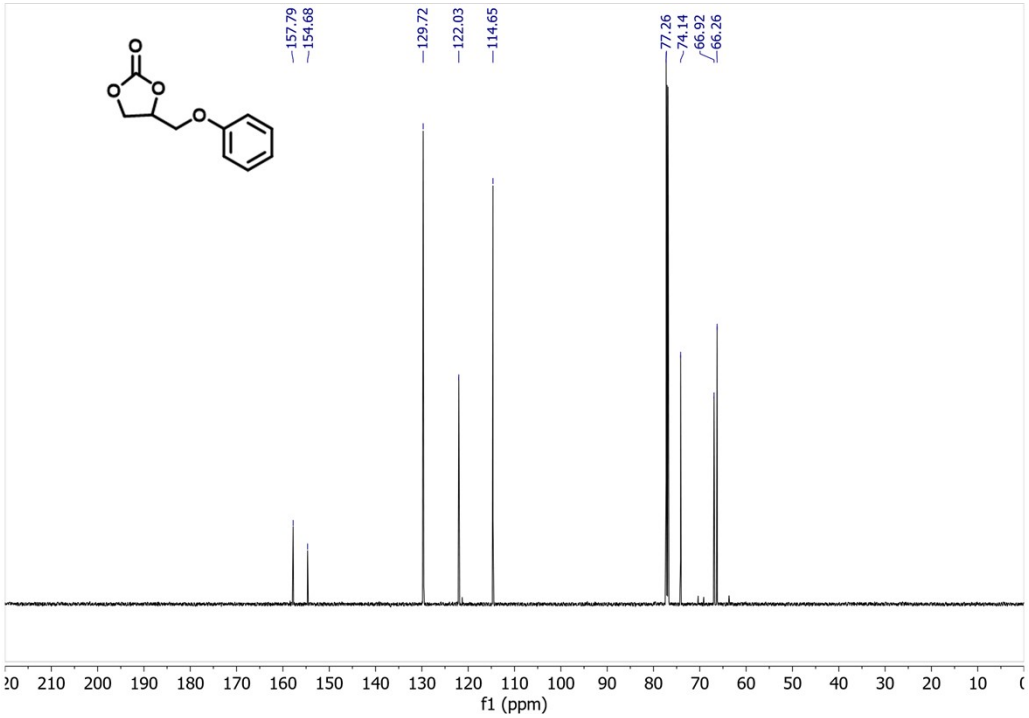

Figure S60. ^{13}C NMR ($CDCl_3$) spectrum of **11b** after chromatographic purification.

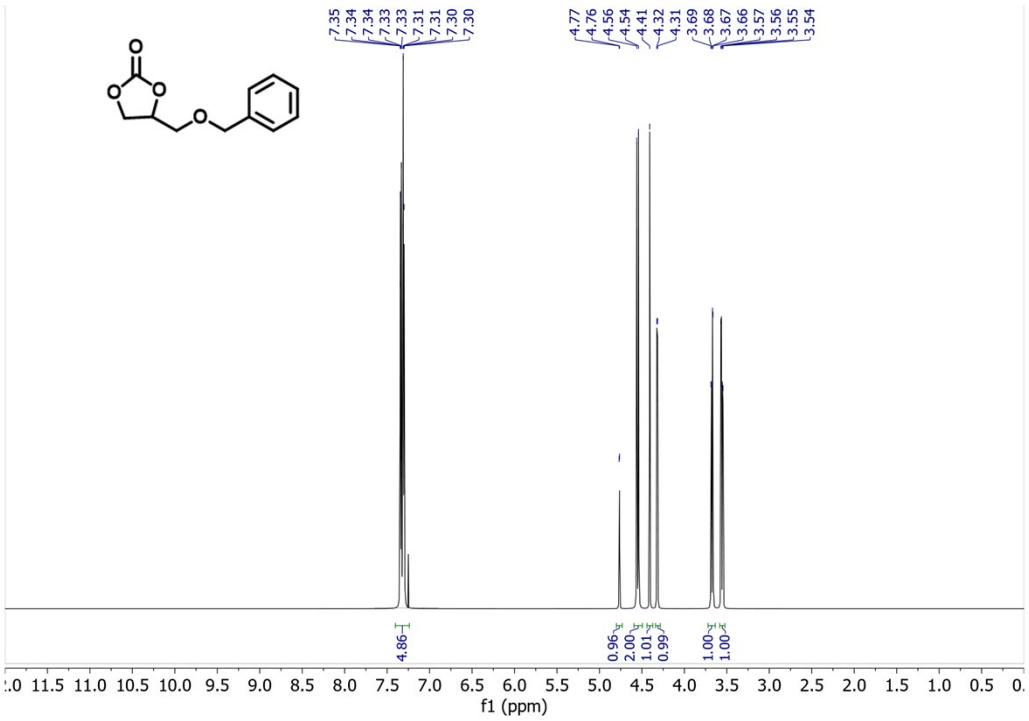

Figure S61. ^{1}H NMR ($CDCl_3$) spectrum of **12b** after chromatographic purification.

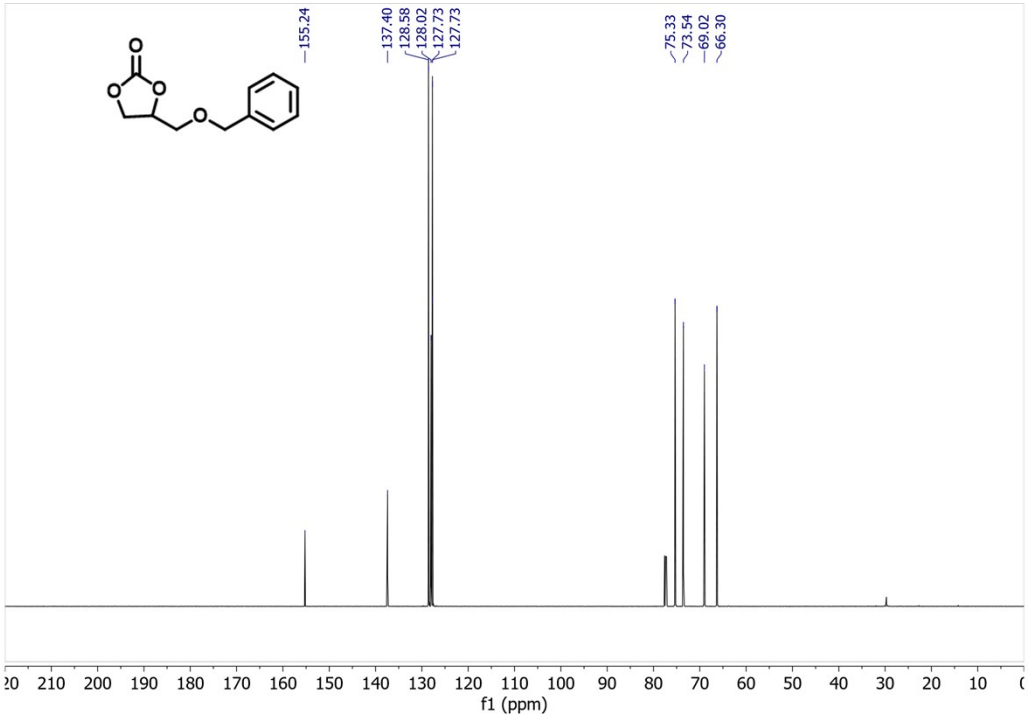

Figure S62. ^{13}C NMR ($CDCl_3$) spectrum of **12b** after chromatographic purification.

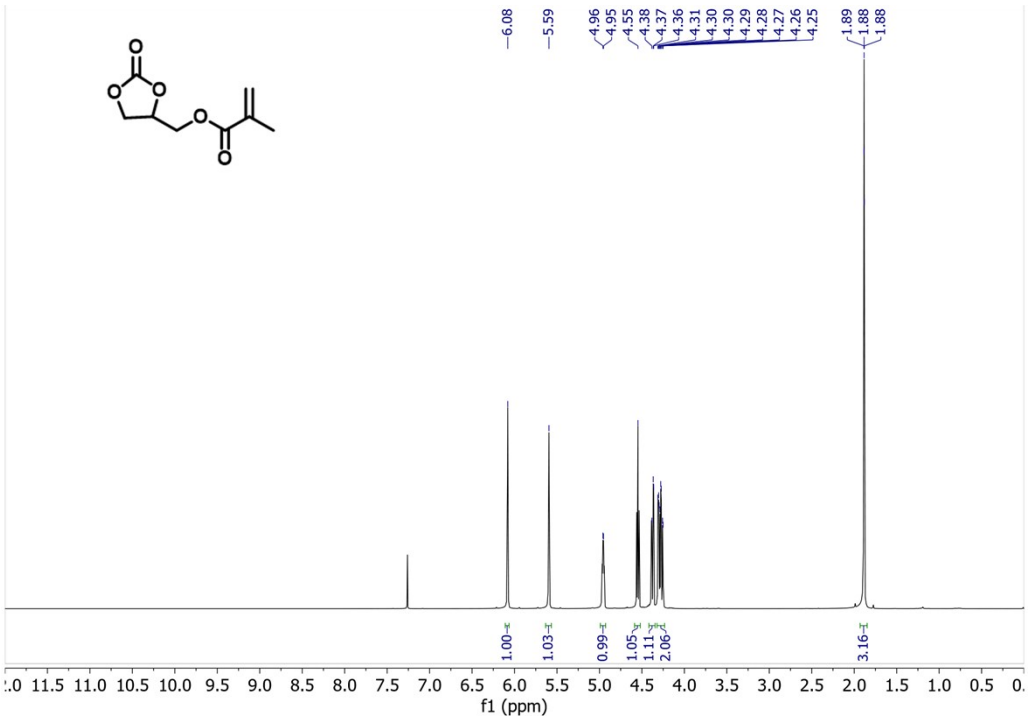

Figure S63. ^{1}H NMR ($CDCl_3$) spectrum of **13b** after chromatographic purification.

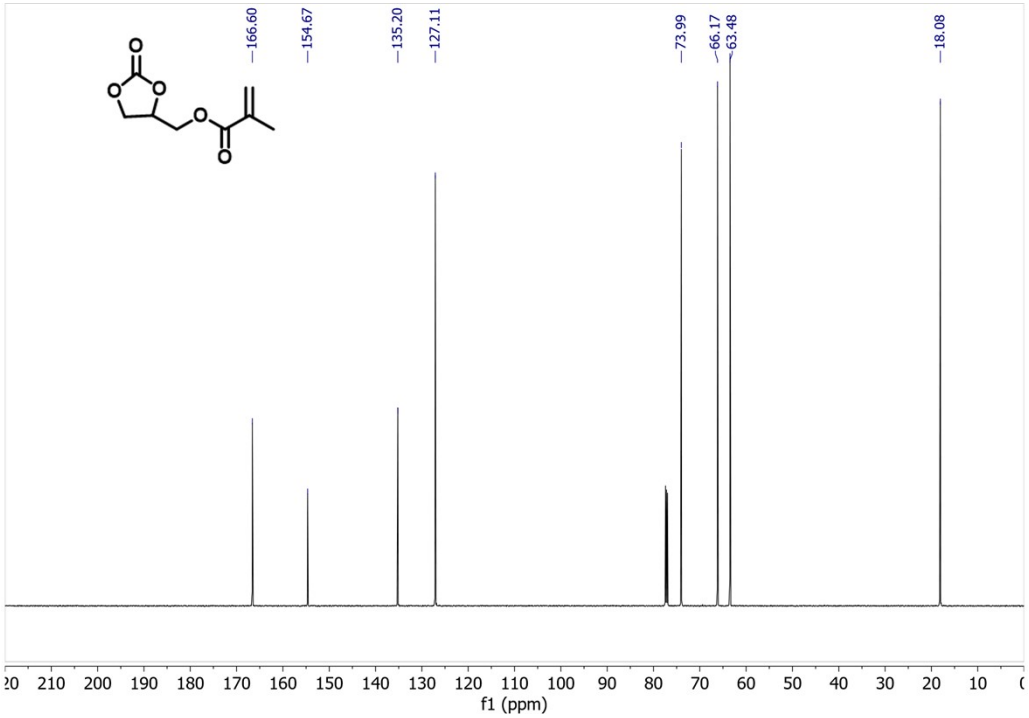

Figure S64. ^{13}C NMR ($CDCl_3$) spectrum of **13b** after chromatographic purification.

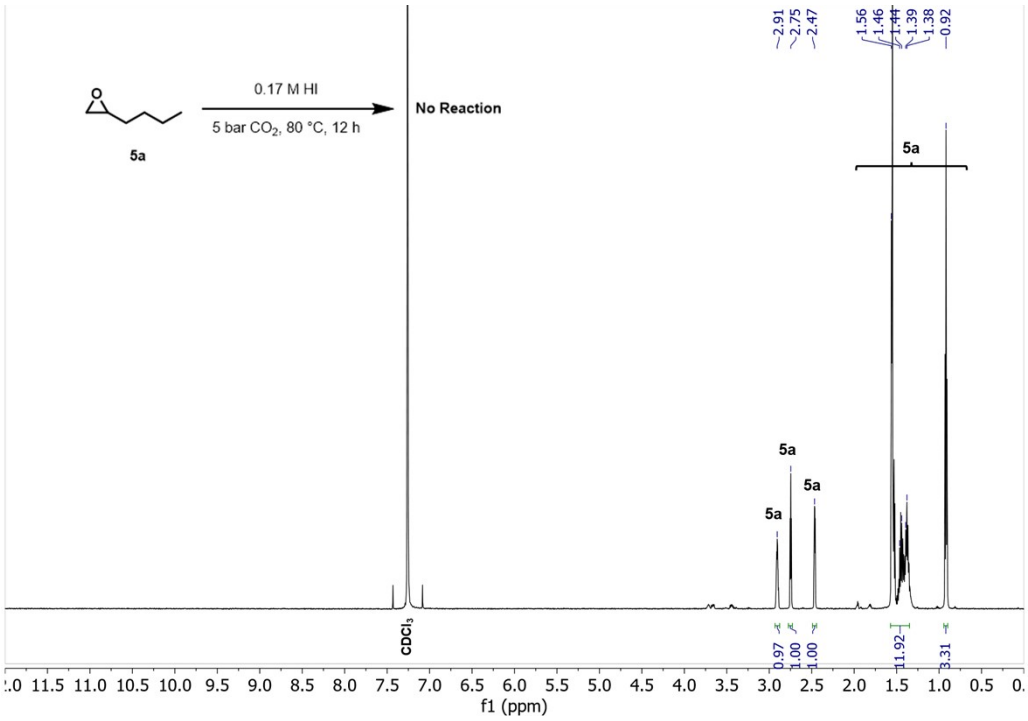

Figure S65. Crude ^{1}H NMR ($CDCl_3$) spectrum of cycloaddition of CO_2 to **5a** substrate by using 0.5 mL of 0.17 M HI, 5 bar CO_2, 80 °C, 12 h; **Table S2, Entry 1**

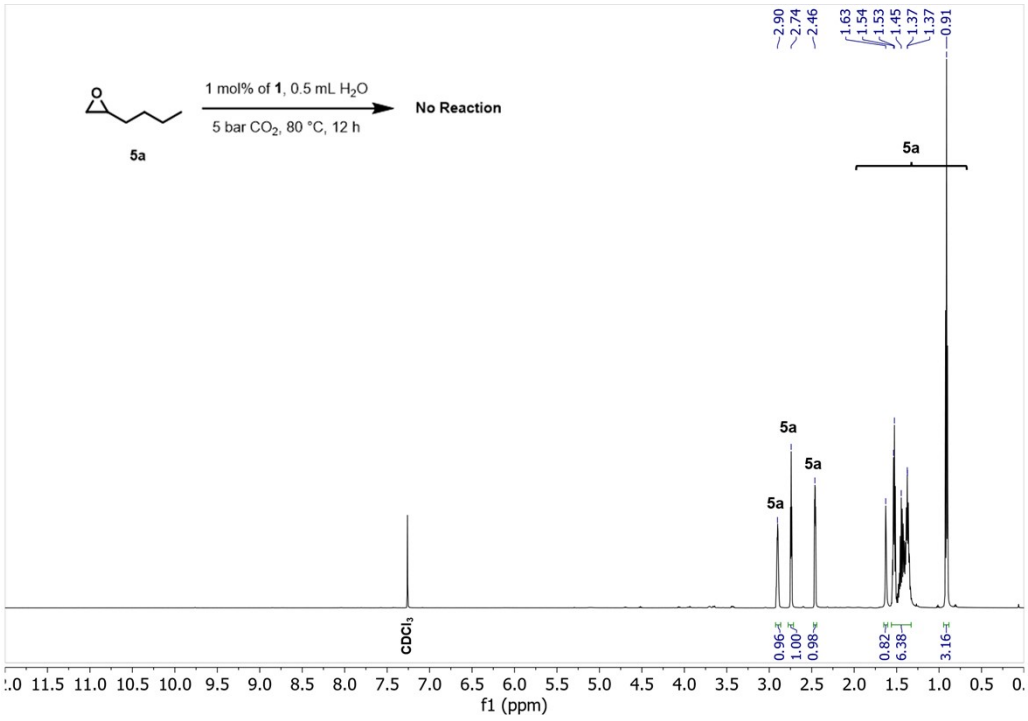

Figure S66. Crude ^{1}H NMR ($CDCl_3$) spectrum of cycloaddition of CO_2 to **5a** substrate by using 1 mol% of **1**, 0.5 mL of H_2O, 5 bar CO_2, 80 °C, 12 h; **Table S2, Entry 2**

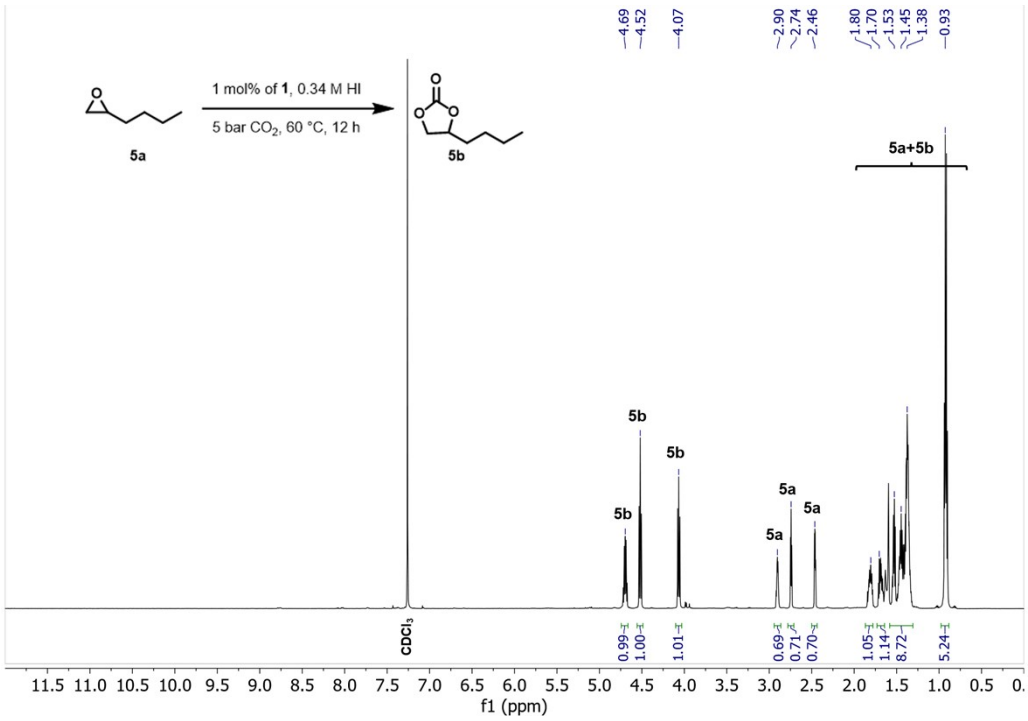

Figure S67. Crude ^{1}H NMR ($CDCl_3$) spectrum of cycloaddition of CO_2 to **5a** substrate by using 1 mol% of **1**, 0.25 mL of 0.34 M HI, 5 bar CO_2, 60 °C, 12 h; **Table S2, Entry 4**

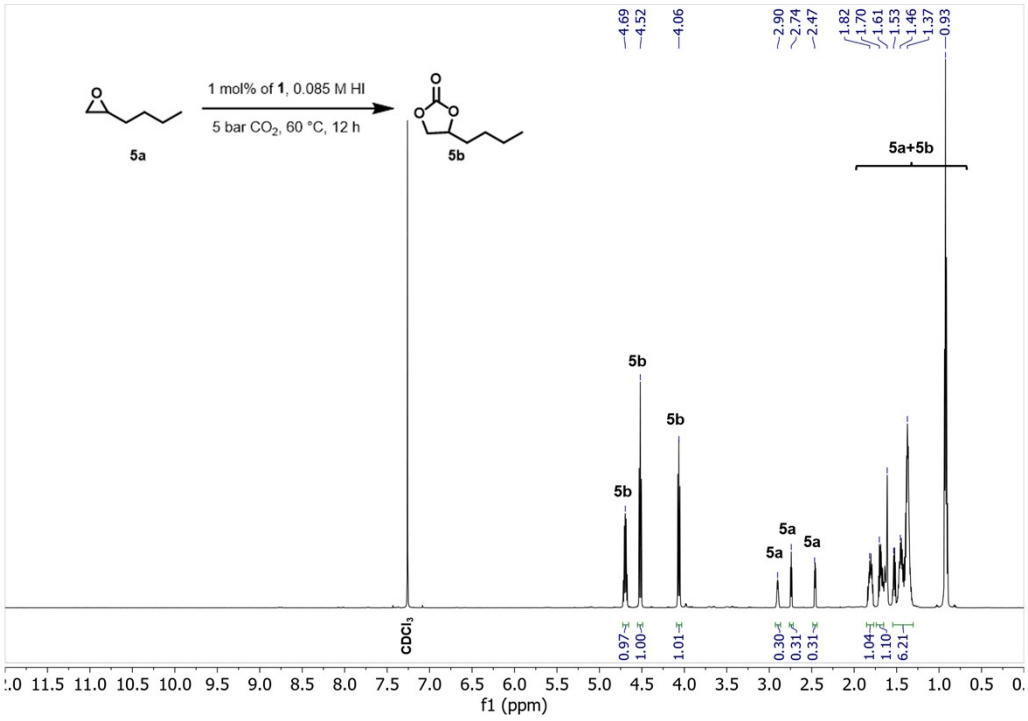

Figure S68. Crude ^{1}H NMR ($CDCl_3$) spectrum of cycloaddition of CO_2 to **5a** substrate by using 1 mol% of **1**, 1.00 mL of 0.085 M HI, 5 bar CO_2, 60 °C, 12 h; **Table S2, Entry 6**

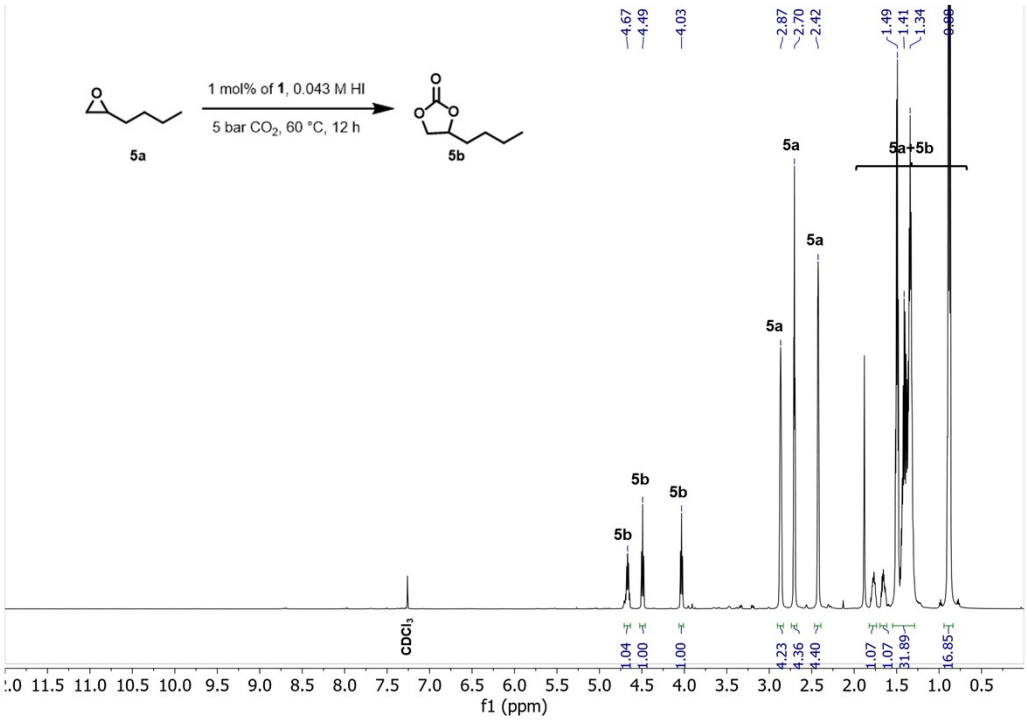

Figure S69. Crude ^{1}H NMR ($CDCl_3$) spectrum of cycloaddition of CO_2 to **5a** substrate by using 1 mol% of **1**, 2.00 mL of 0.043 M HI, 5 bar CO_2, 60 °C, 12 h; **Table S2, Entry 7**

S8. Analysis of phases of the reaction mixture and mass balance

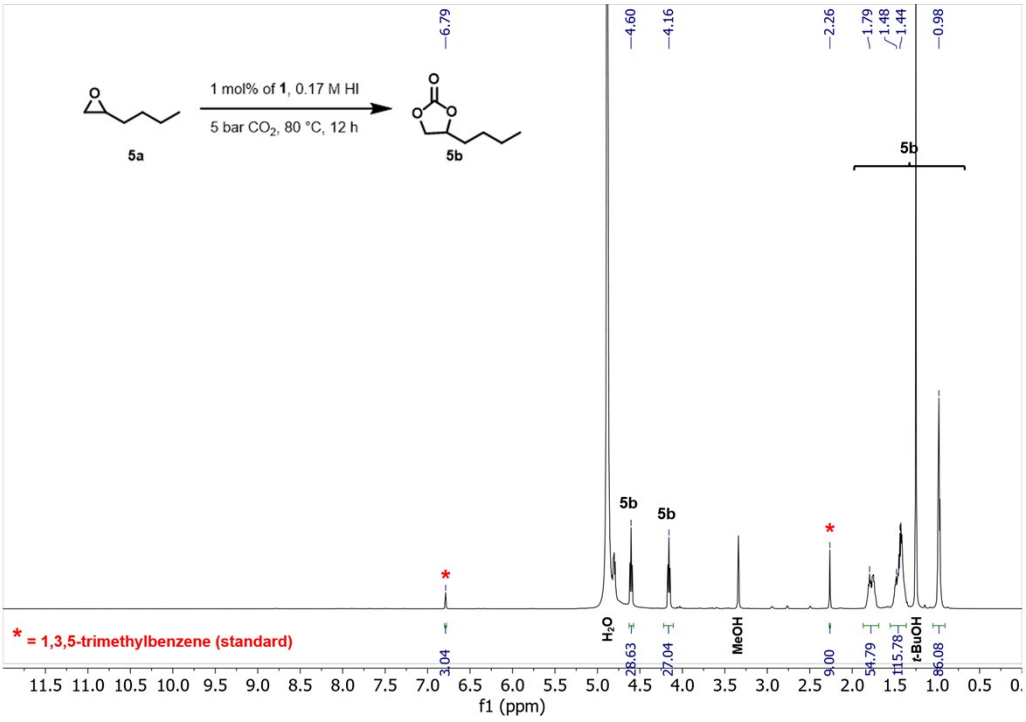

Figure S70. ^{1}H NMR (MeOD) spectrum of the organic phase from the cycloaddition of CO_2 to **5a** (8.33 mmol). Amount of **5b**: 8.23 mmol; mass balance (8.23/8.33)= 98.8%.

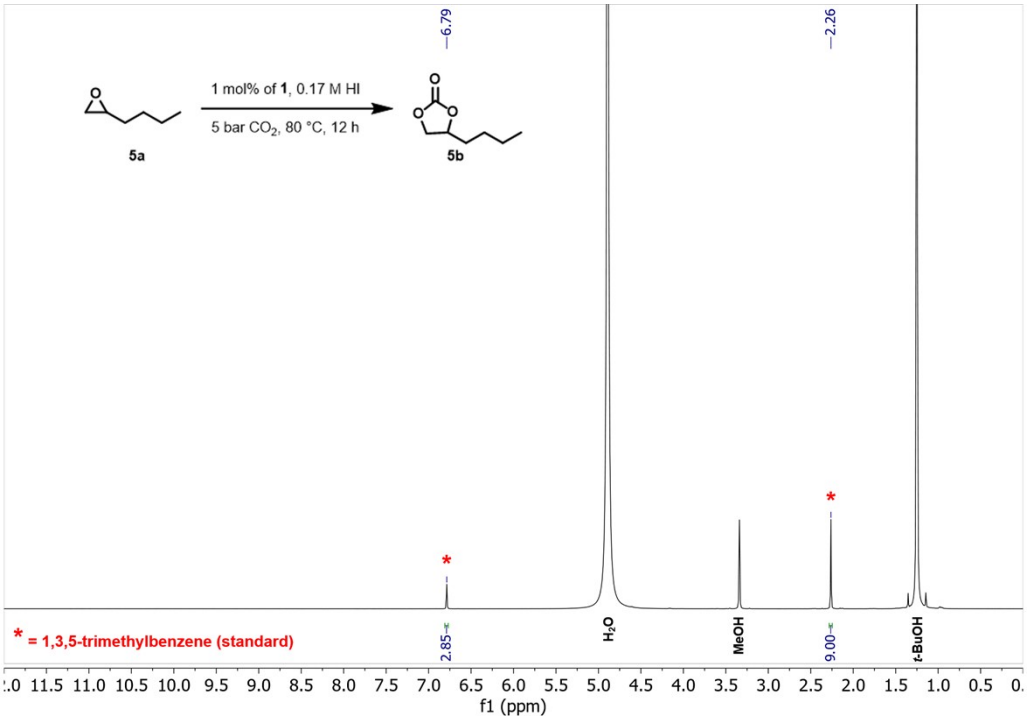

Figure S71. ^{1}H NMR (MeOD) spectrum of the aqueous phase from the cycloaddition of CO_2 to **5a**; no organic products were detected.

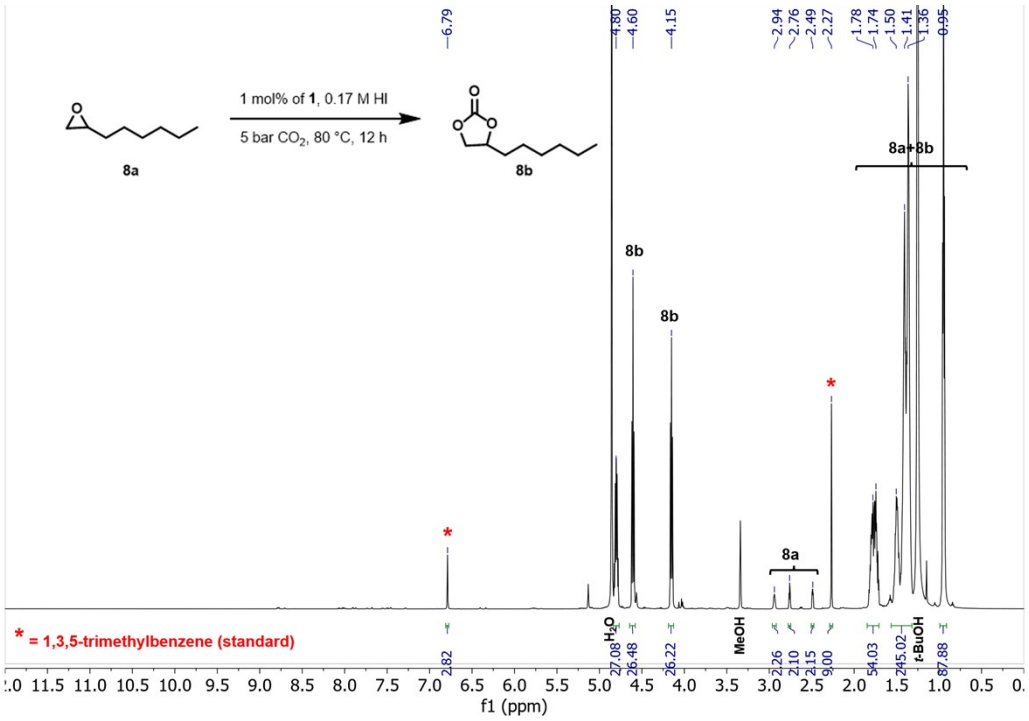

Figure S72. ^{1}H NMR (MeOD) spectrum of the organic phase from the cycloaddition of CO_2 to **8a** (8.33 mmol). Amount of **8b**: 7.61 mmol; amount of **8a**: 0.61 mmol, mass balance (8.22/8.33)= 98.7%.

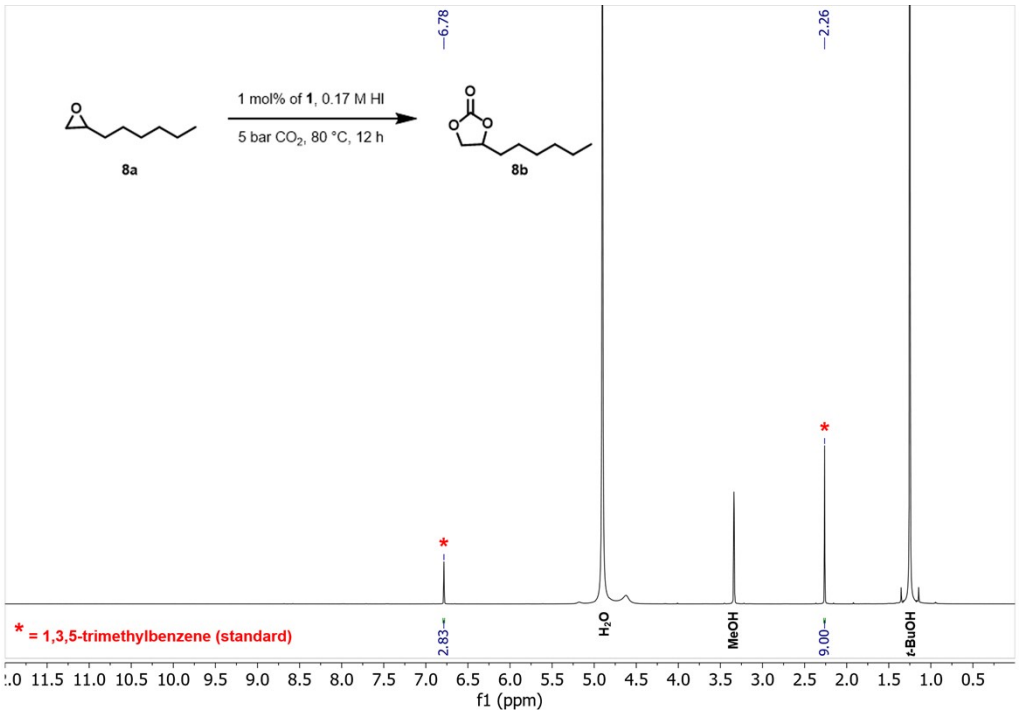

Figure S73. ^{1}H NMR (MeOD) spectrum of the aqueous phase from the cycloaddition of CO_2 to **8a**; no organic products were detected.

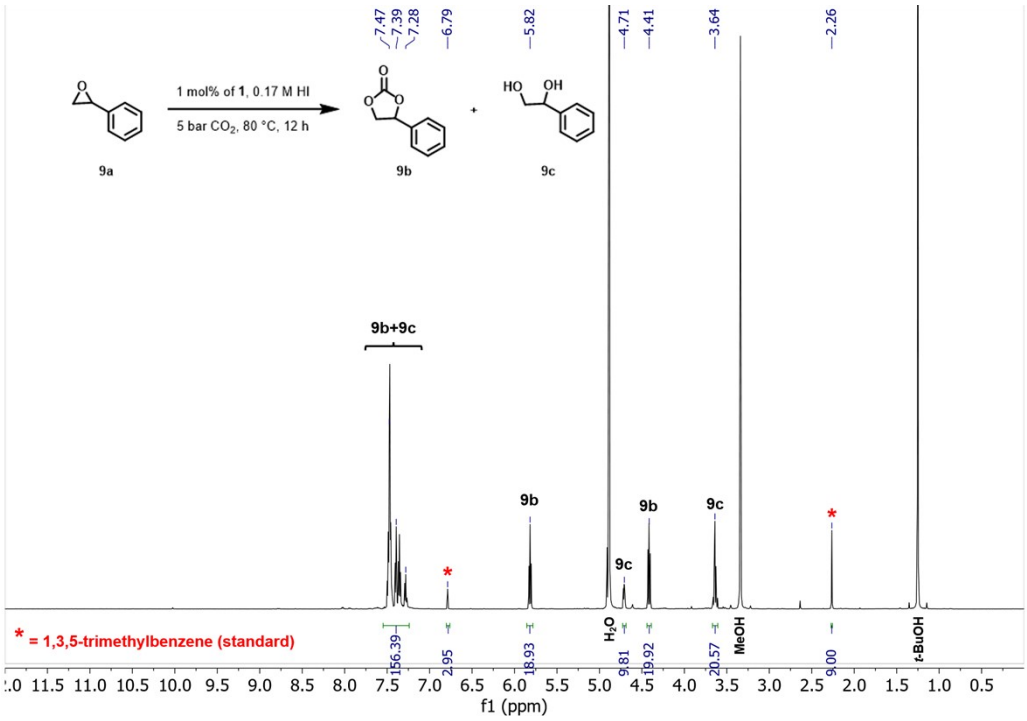

Figure S74. ^{1}H NMR (MeOD) spectrum of the organic phase from the cycloaddition of CO_2 to **9a** (8.33 mmol). Amount of **8b**: 7.61 mmol; amount of **8a**: 0.61 mmol, mass balance (8.22/8.33)= 98.7%.

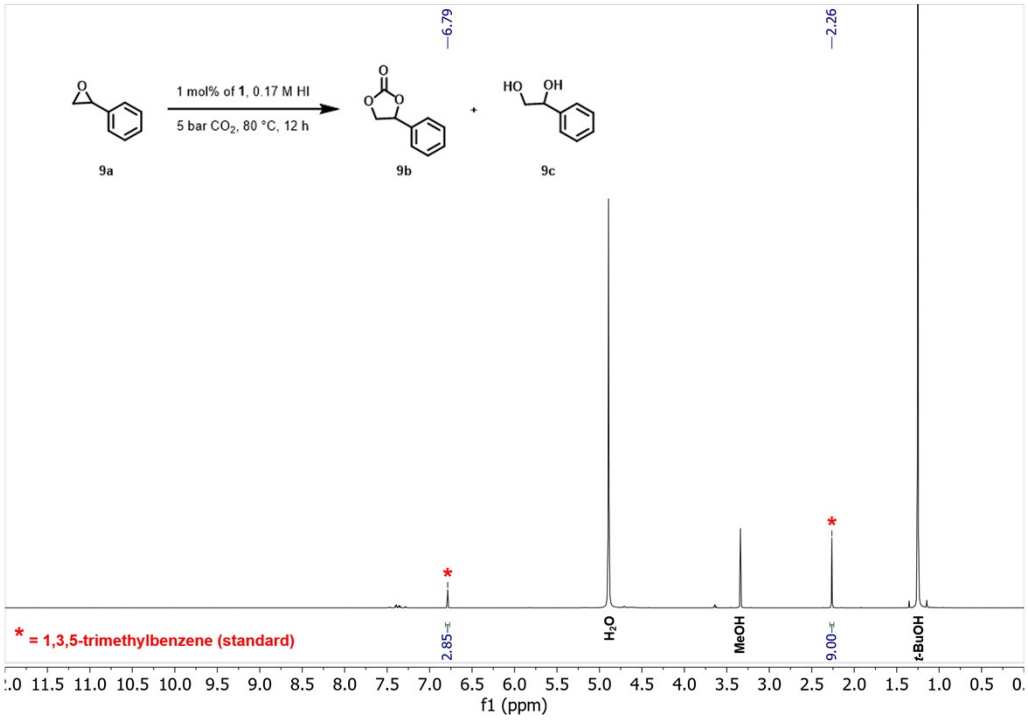

Figure S75. ^{1}H NMR (MeOD) spectrum of the aqueous phase from the cycloaddition of CO_2 to **9a**; no organic products were detected.

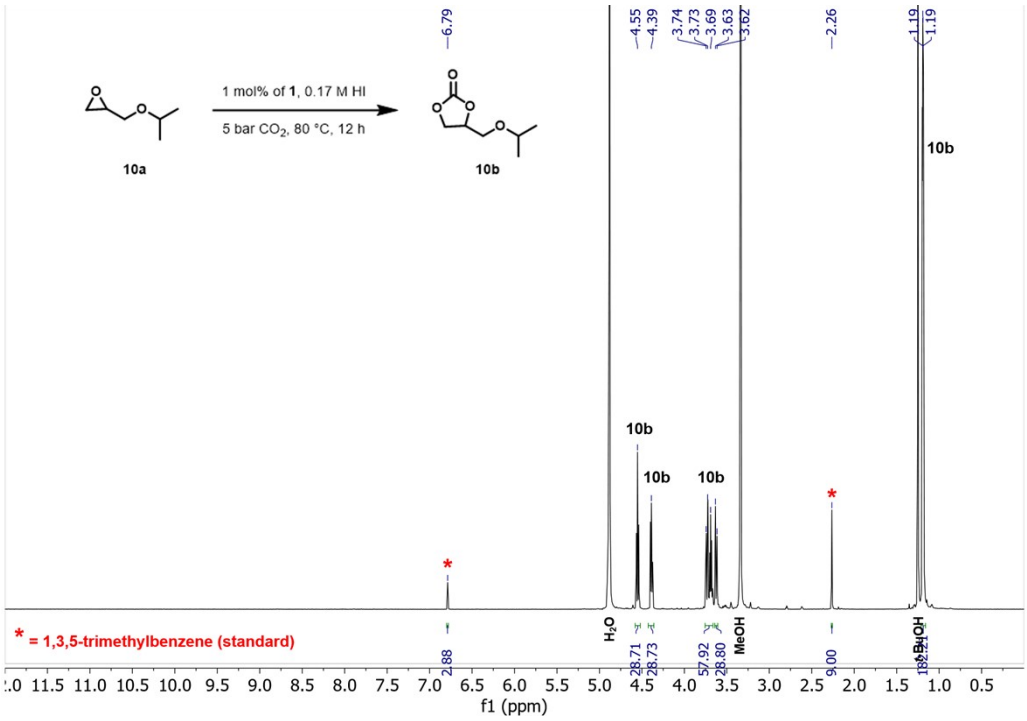

Figure S76. ^{1}H NMR (MeOD) spectrum of the organic phase from the cycloaddition of CO_2 to **10a** (8.33 mmol). Amount of **5b**: 8.26 mmol; mass balance (8.26/8.33)= 99.2%.

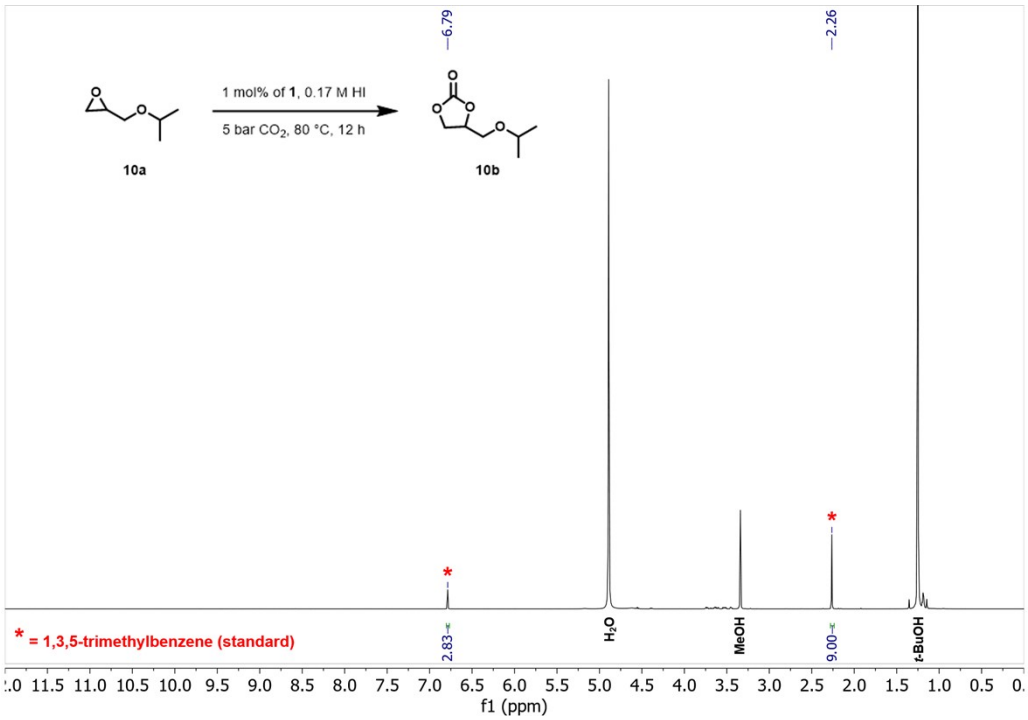

Figure S77. ^{1}H NMR (MeOD) spectrum of the aqueous phase from the cycloaddition of CO_2 to **10a**; no organic products were detected.

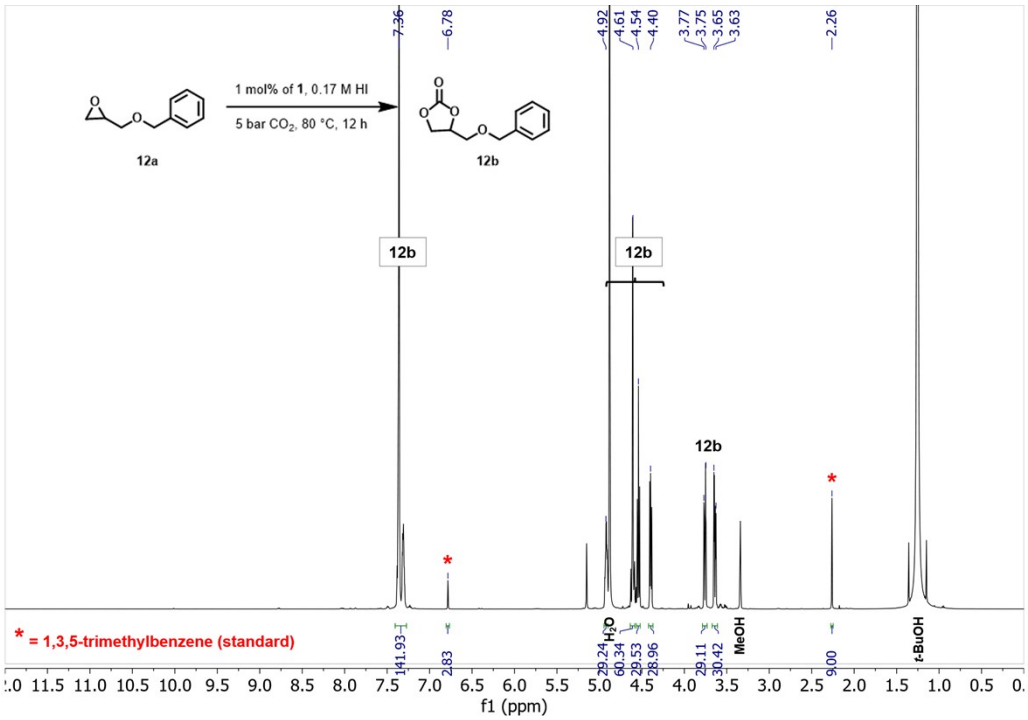

Figure S78. ^{1}H NMR (MeOD) spectrum of the organic phase from the cycloaddition of CO_2 to **12a** (8.33 mmol). Amount of **12b**: 8.33 mmol; mass balance: 99.9%

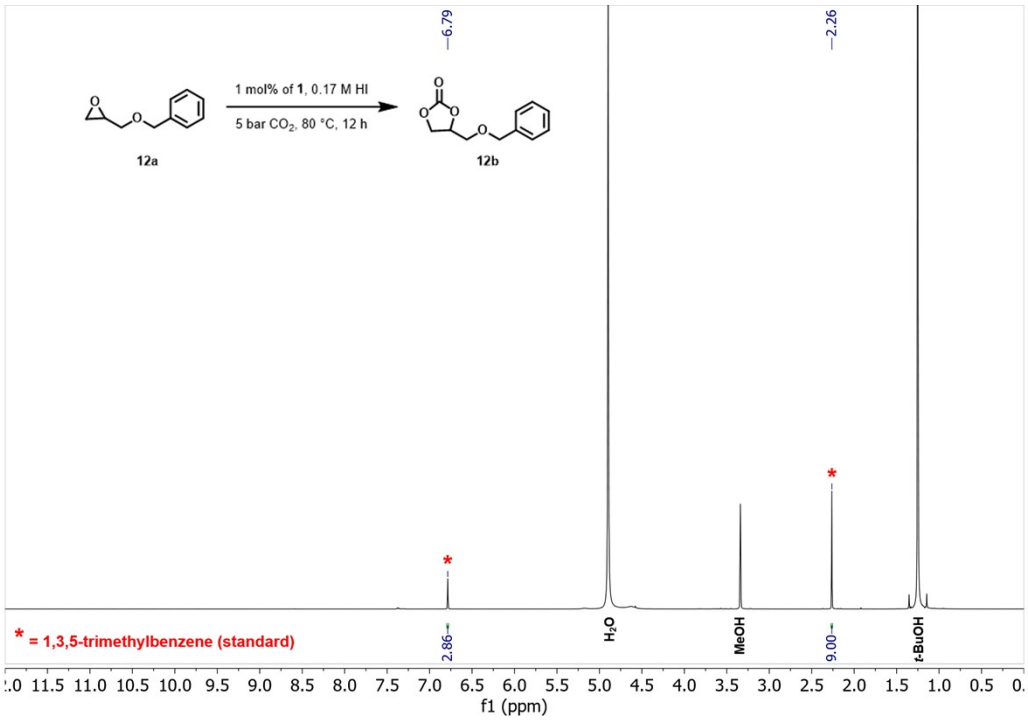

Figure S79. ^{1}H NMR (MeOD) spectrum of the aqueous phase from the cycloaddition of CO_2 to **12a**; no organic products were detected.

S9. Supporting references

1. J. Poolwong, V. Aomchad, S. Del Gobbo, A. W. Kleij and V. D'Elia, *ChemSusChem*, 2022, **15**, e202200765.
2. A. Mitra, S. Ghosh, K. S. Paliwal, S. Ghosh, G. Tudu, A. Chandrasekar and V. Mahalingam, *Inorganic Chemistry*, 2022, **61**, 16356-16369.
3. S. Saengsaen, S. Del Gobbo and V. D'Elia, *Chemical Engineering Research and Design*, 2023, **191**, 630-645.
4. Q. Thi Nguyen, Y. Bae, X. H. Do, S. H. Kim, J. Na, K.-Y. Baek and Y.-R. Lee, *Energy & Fuels*, 2024, **38**, 7097-7107.
5. J. Chen, G. Chiarioni, G.-J. W. Euverink and P. P. Pescarmona, *Green Chemistry*, 2023, **25**, 9744-9759.
6. C. Guo, G. Chen, N. Wang, S. Wang, Y. Gao, J. Dong, Q. Lu and F. Gao, *Separation and Purification Technology*, 2023, **312**, 123375.
7. Z. Yue, T. Hu, H. Su, W. Zhao, Y. Li, H. Zhao, Y. Liu, Y. Liu, H. Zhang, L. Jiang, X. Tang, S. Shan and Y. Zhi, *Fuel*, 2022, **326**, 125007.